Petrogenesis of the Ophiolitic Giant Chromite Deposits of Kempirsai, Kazakhstan: a Study of Solid and Fluid Inclusions in Chromite

Article *in* Journal of Petrology · October 1997

DOI: 10.1093/petrology/38.10.1419

CITATIONS
364

READS
778

5 authors, including:

Frank Melcher
Montanuniversität Leoben
188 PUBLICATIONS **3,924** CITATIONS

SEE PROFILE

JOURNAL OF PETROLOGY | VOLUME 38 | NUMBER 10 | PAGES 1419–1458 | 1997

Petrogenesis of the Ophiolitic Giant Chromite Deposits of Kempirsai, Kazakhstan: a Study of Solid and Fluid Inclusions in Chromite

FRANK MELCHER*, WALTER GRUM, GRIGORE SIMON†, TATIANA V. THALHAMMER AND EUGEN F. STUMPFL

INSTITUTE OF GEOLOGICAL SCIENCES, UNIVERSITY OF LEOBEN, 8700 LEOBEN, AUSTRIA

RECEIVED 3 MAY, 1996; REVISED TYPESCRIPT ACCEPTED 9 JUNE, 1997

Chromites forming giant orebodies in the southern part of the Early Palaeozoic ophiolite sequence of the Kempirsai Massif (Kazakhstan, Urals) contain a large number of inclusions, i.e. silicates, sulphides, alloys, arsenides, and fluids. The chromite orebodies are surrounded by dunite envelopes of variable thickness, which show transitional boundaries to harzburgite host rocks. The composition of ore-forming chromites in depleted mantle rocks of the southern part of the massif (Main Ore Field) is rather uniform, showing high cr*-number [100Cr/(Cr+Al), 78–84] and* mg*-number [100Mg/(Mg+Fe^{2+}), 51–85] values. Smaller bodies of Al-rich spinel in the northern and western part of the massif (Batamshinsk) have variable* cr*-number (38–60) and* mg*-number (50–88) values. Three textural types of inclusions in chromite are distinguished: (1) In Main Ore Field chromites, primary silicate inclusions generally have high* mg*-number (>95), Cr and Ni, and are dominated by pargasitic amphibole, forsterite, diopside, enstatite and Na-phlogopite. Chromite formed over a temperature range from ~1200° to <1000°C at oxygen fugacities 1–2 log units above the fayalite–magnetite–quartz (FMQ) buffer. A diversity of primary and secondary platinum-group minerals (PGM) is described from the chromitites, including alloys, sulphides, sulpharsenides and arsenides of Ru, Os, Ir, Rh, Ni, Cu, Fe and Co. Alloys, sulphides and arsenides free of platinum-group elements are attributed to serpentinization of chromitite. (2) In addition to primary PGM and hydrous silicates, fluid inclusions of up to 50 μm size are frequently included in chromite within chromite–amphibole veins discordant to massive chromitite in the Main Ore Field. The fluids are low to moderately saline, sodium-dominated aqueous solutions with complex gas contents. Variable amounts of water, hydrogen, hydrocarbons, carbon dioxide and nitrogen have been determined in inclusion-rich samples. (3) In the northern and western part of the Kempirsai massif, complex silicate–oxide assemblages formed in small orebodies of orbicular Al-rich chrome spinel. Chlorite, amphibole, hydrogarnet, sphene, manganoan ilmenite and Ca–Ti oxide are documented in addition to Ni sulphides and rare PGM. The formation of chromitite in the Kempirsai Massif is explained in terms of a multi-stage process involving mantle fluids. Low-Cr, high-Al spinel present in small orebodies in the northern and western part of the massif formed from mid-ocean ridge basalt (MORB)-type melts extracted from fertile mantle in an extensional tectonic setting. The large orebodies and the amphibole–chromite veins in the southern part formed later from interaction of hydrous, second-stage high-Mg melts and fluids with depleted mantle in a convergent tectonic setting. Metasomatic alteration of the mantle wedge above subducted crust by fluids played an important role in generating second-stage melts and in releasing metals.*

KEY WORDS: *chromite; Kempirsai ophiolite; Urals; platinum-group minerals; fluids*

INTRODUCTION

Large chromite deposits (>10 Mt chromite) of ophiolitic affinity are rare. To date, podiform chromite 'giants'

*Corresponding author.

† Present address: Department of Geological Sciences, University of Michigan, Ann Arbor, MI 48109, USA.

(>100 Mt chromite) are known only from the Kempirsai district, Kazakhstan. In addition to high-grade chromite ore, podiform chromite deposits usually carry low-grade mineralizations of platinum-group elements (PGE) (e.g. Stockman & Hlava, 1984; Talkington *et al.*, 1984; Legendre & Augé, 1986; Prichard *et al.*, 1986, 1994; Augé, 1988; Augé & Johan, 1988; Orberger *et al.*, 1988; McElduff & Stumpfl, 1990; Tarkian *et al.*, 1991; Yang & Seccombe, 1993). Kempirsai is the largest ultramafic massif in the southern Urals and contains exceptionally large orebodies of podiform chromite. It forms part of a Palaeozoic ophiolite belt extending in a north–south direction along the Ural mountain chain (Heraskov & Razumova, 1967; Pavlov *et al.*, 1968; Kamaletdinov, 1974; Perfiliev, 1979). Giant orebodies of Cr-rich chromitite reaching up to 1500 m in length and 100–150 m in thickness are located in highly depleted harzburgitic and dunitic mantle rocks. Kazakhstan thus is the world's number two producer, after South Africa, of chromite ore and ferrochrome alloys. Production in 1994 was 2 million tons, of which >50% was exported. Maximum PGE contents in chromitites exceed 1 p.p.m. and are dominated by Ir, Ru and Os (Volchenko & Vigorov, 1987; Distler *et al.*, 1989; Dmitrenko, 1994; Melcher *et al.*, 1994). Taking into account the total reserves of chromite ores (>300 Mt in the southern part alone), the reserves of PGE can be estimated at 240 tons (Distler *et al.*, 1989). A diversity of explanations for the origin of podiform chromite deposits has been postulated (e.g. Irvine, 1967; Thayer, 1969; Malpas & Strong, 1975; Lago *et al.*, 1982; Johan *et al.*, 1983; Stowe, 1987; Paktunç, 1990; Zhou *et al.*, 1994, 1996). In most genetic concepts, processes such as multi-stage melting of upper mantle, melt segregation, magma mixing and melt–rock interaction play an important role. Magmas of picritic or boninitic affinity are generally believed to be parental to high-Cr chromite. From such magmas, large volumes of chromite and olivine may fractionate (Roberts, 1988). Investigations of inclusions in chromite of podiform chromitite within the past 20 years have added a new dimension to our understanding of chromitite genesis in mantle tectonites and cumulates of ophiolitic settings. Evidence obtained from both the hydrous nature of many inclusions (amphiboles, phlogopite, fluids) and the mineral chemistry, which is different from that of the matrix surrounding chromites, has resulted in a number of models which attempt to explain these features by interaction of fluids with magma (Johan *et al.*, 1983), and the idea of metasomatic origin for dunites associated with chromitites. Important aspects of inclusions in chromite have been discussed by, among others, Stockman & Hlava (1984), Talkington *et al.* (1984), Johan (1986), Legendre & Augé (1986), Prichard *et al.* (1986, 1994), Augé (1987, 1988), Augé & Johan (1988), Lorand & Ceuleneer (1989), Ferrario & Garuti (1990), McElduff & Stumpfl (1990, 1991), Nilsson (1990), Thalhammer *et al.* (1990) and Torres-Ruiz *et al.* (1996). Within many ultramafic complexes, fluids may play an important role in the formation of chromitite (Johan *et al.*, 1983; Johan, 1986; Augé, 1987; Lorand & Ceuleneer, 1989; Ferrario & Garuti, 1990), and in transporting and precipitating PGE (Volborth *et al.*, 1985; Ballhaus & Stumpfl, 1986; Boudreau *et al.*, 1986; Stumpfl, 1986, 1993; Ballhaus *et al.*, 1988; Mathez, 1989; Ferrario & Garuti, 1990; Mogessie & Saini-Eidukat, 1992; Evstigneeva & Tarkian, 1996). Much of this evidence is based on the study of mineral inclusions in chromite. In this paper we present a complete data set on solid and fluid inclusions in ore-forming chromite of the large podiform deposit of Kempirsai. Detailed investigations of isotope systematics and of fluid compositions have been published elsewhere (Melcher *et al.*, 1996, 1997; Thalhammer, 1996*a*,*b*; Melcher *et al.*, in preparation). The role of fluids in the formation of chromite and associated minerals is critically evaluated.

GEOLOGICAL SETTING

The Kempirsai ultramafic massif is situated within the Sakmara Allochthon of the Central Ural Uplift. It represents the southernmost part of the Palaeozoic Western Ophiolite Belt, extending over 2000 km in a north–south direction. The Sakmara Allochthon overlies to the west the West Uralian zone (shelf sediments) and is bounded to the east by the Main Ural Deep-fault. East of that fault, units of the Magnitogorsk island-arc are exposed, which are overthrust by Precambrian to Early Palaeozoic microcontinents (Zonenshain *et al.*, 1984). Uralian ophiolites underwent a complex evolution in the Uralian palaeo-ocean. An early continental rifting event in the Lower Ordovician was followed by an epoch of spreading and formation of oceanic crust in the Middle Ordovician–Lower Silurian, with development of island-arc volcanism as early as Middle Ordovician. Intra-oceanic thrusts within the oceanic crust of the Sakmara Zone eventually developed into subduction zones (Savelieva & Nesbitt, 1996) dipping eastward underneath the Magnitogorsk island arc. The Sakmara Allochthon contains sedimentary and metamorphic sequences, which form part of the Uraltau anticlinorium. Between the ophiolite massifs and the Main Ural fault, a narrow belt of metasediments and meta-ophiolites including eclogite-facies assemblages is exposed. The best known of these is the north–south trending Maksyutov Complex, situated ~50 km north of Kempirsai (Lennykh *et al.*, 1995). There, eclogites record metamorphic peak conditions of 27 kbar and 615°C (Beane *et al.*, 1996*a*; Dobretsov *et al.*, 1996). Kempirsai is the largest ultramafic massif in the southern Urals and has been obducted, together with the Sakmara Allochthon, onto the Eastern European platform during

the Uralian orogeny (Pavlov *et al.*, 1968; Edwards & Wasserburg, 1985). The general features of the massif, its tectonic position and its magmatic sequence have been described by Sokolov (1948), Pavlov *et al.* (1968), Segalovich (1973), Smirnova (1973), Laz'ko (1989), and Saveliev & Savelieva (1991).

The Kempirsai massif, covering an area of 2000 km^2, is of elongated shape with a long axis of 90 km trending north–south and is up to 32 km wide in an east–west direction (Fig. 1). The magmatic stratigraphy comprises a complete ophiolite sequence, ranging from fertile mantle to depleted mantle harzburgite tectonites (including chromitites), cumulates, a sheeted dyke complex, lava flows and ocean-floor sediments. The massif consists of two parts, separated by a north–south trending shear zone (Pavlov *et al.*, 1968; Segalovich, 1973), which is related to the Main Ural fault (Lennykh *et al.*, 1995).

(1) The southeastern part, called the Main Ore Field (MOF), hosts the main chromite deposits and comprises dunite, harzburgite and harzburgite with rare layers of lherzolite, reaching a total thickness of 16 km (Segalovich, 1973). Pyroxenite veins occur throughout the mantle stratigraphy of the MOF. Massive chromite orebodies are frequently cross-cut by chromite-bearing amphibole veins. The main structures are: a NNE–SSW trending anticline, the hinge line of which can be traced over 22 km; an axial-plane fault parallel to the hinge line; and several nearly east–west trending faults. The podiform chromitites are situated on both sides of the anticline and form vein-like, pencil-shaped, flattened bodies. Their long axis is generally parallel to the foliation visible in the host rocks (Kravchenko & Grigoryeva, 1986). They are characteristically enveloped by dunite shells of variable thickness. The largest chromite deposits in the western part of the syncline are the Millionnoe, Diamond Pearl and 20 Years of Kazakh SSR deposits, dipping 5–50° to the west (Pavlov *et al.*, 1968). The eastern part of the syncline contains small deposits such as Sputnik, and large deposits such as Mir, Voskhod–Karagash and 40 Years of Kazakh SSR–Molodezhnoe; these orebodies dip 15–75° to the east. Orebodies are frequently dismembered by east–west trending high-angle faults. A group of large orebodies in the southernmost part of the MOF contains reserves of 310 Mt chromite ore averaging 50 wt % Cr_2O_3, from which about 30 Mt have already been mined (G. Elpashev, personal communication, 1993). The largest orebodies reach 1800 m in length (Molodezhnoe) and 230 m in thickness (Diamond Pearl).

(b) The general stratigraphy of the northern and western part of the Kempirsai Massif comprises dunites and harzburgites in the lower part of the section, overlain by a crustal sequence of ultramafic and mafic cumulates. The uppermost portion of the ophiolite complex, e.g. the sheeted dyke complex, basalts and marine sediments, is exposed at the southwestern edge of the massif. The entire sequence has a thickness of up to 5 km (Segalovich, 1973). Al-rich podiform chromitites of much smaller size (up to 100 m in length) than those in the southern part occur within harzburgites of the mantle section in the Tagashasai and Batamshinsk ore fields (e.g. orebody 117; Fig. 1). They are also rimmed by dunites and referred to as the Batamshinsk-type chromite ores (BAT). The mantle sequence and the cumulates are frequently transected by gabbroic dykes.

Apart from typical podiform chromitites hosted by depleted mantle rocks, there is a second stratigraphic level of chromite mineralization in the western part of the Kempirsai Massif. Small (a few tens of metres long, 3–5 m thick), Cr-poor, Al-rich orebodies occur at, or close to, the inferred crust–mantle boundary in the southwestern part of the massif near the village of Stepninsk (Fig. 1). Because of the chemical similarities of Batamshinsk-type chromites and those at Stepninsk (Pavlov & Grigoryeva, 1977), all chromitites in the northern and western part of the massif are referred to as Batamshinsk-type chromite ores (BAT).

The metamorphic history of ultramafic rocks in the Kempirsai Massif has not been studied in any detail. The mantle rocks underwent high-temperature recrystallization and deformation processes within the mantle; no regional metamorphic event occurred before obduction-related serpentinization. The ultramafic rocks of the MOF at Kempirsai have experienced serpentinization of variable intensity. In drillcores (DH 639; Fig. 1), serpentinization rapidly increases uphole. Serpentinization affects only the grain boundaries of olivine and orthopyroxene below a depth of 1300 m; above 1000 m, most of the ultramafic rocks are completely serpentinized. Chromite orebodies located close to the surface are invariably hosted by serpentine minerals + brucite; the intensity of late-tectonic brecciation also increases towards the surface. Massive gel-type magnesite overlies large portions of the ore-bearing zone.

ANALYTICAL TECHNIQUES

Samples were collected from drillcores and outcrops within the southern and southwestern part of the Kempirsai massif in 1992 and 1993. Mineral compositions were determined by energy- and wavelength-dispersive electron microprobe techniques using an ARL-SEMQ probe at the Institute of Geological Sciences, Leoben. Additional analyses have been performed at the Institute of Mineralogy and Petrology, Innsbruck (ARL-SEMQ microprobe); at IGEM, Moscow (electron microscope); and at the University of Adelaide (CAMECA SX 50

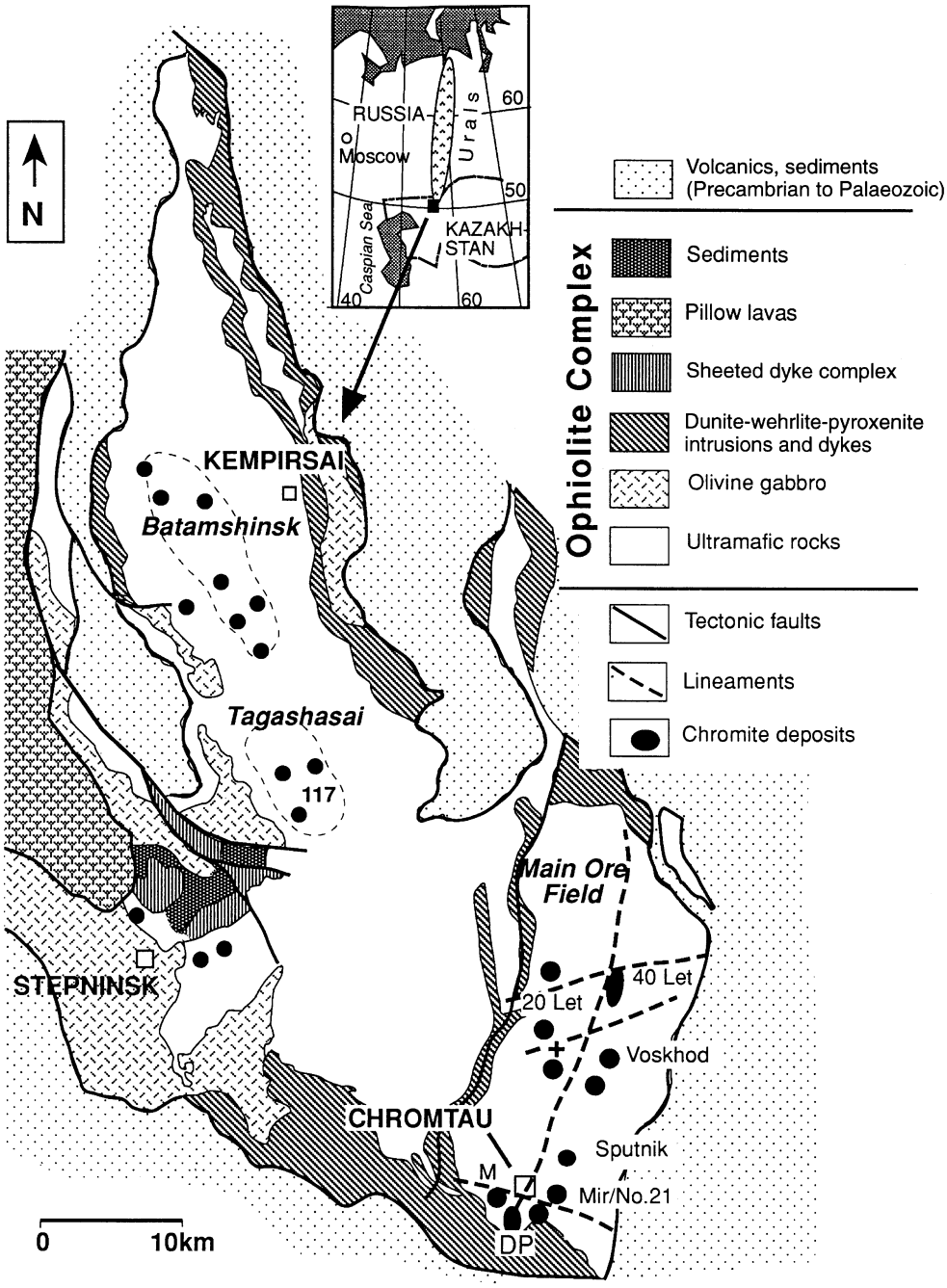

Fig. 1. Geological sketch map of the Kempirsai Massif, modified from Saveliev & Savelieva (1991). DP, Diamond Pearl; M, Millionnoe; 20 Let, 20 Years of Kazakh SSR; 40 Let, 40 Years of Kazakh SSR and Molodezhnoe mines; 117, orebody in the Tagashasai ore field; +, position of drillhole 639, as discussed in the text. Inset map shows position of the Kempirsai Massif, Kazakhstan, in the southernmost Urals.

microprobe). Natural minerals (chromite, olivine, kaersutite, biotite, rhodonite, arsenopyrite, pyrrhotite, millerite, chalcopyrite) and pure metals (Ru, Os, Ir, Rh, Pt, Pd, Cu, Ni, Co) were used as standards. For wavelength-dispersive analysis the microprobe was operated at an acceleration potential of 15 and 20 kV, a beam current of 15 and 20 nA, and a beam diameter of ~1 μm. For the analysis of platinum-group elements at Leoben, the following X-ray lines were used: SKα, FeKα, NiKα, CuKα, CoKα, AsLα_{1+2}, OsMβ, IrLα_1, RuLα_1, RhLα.

Corrections were made for the observed interferences Ru→As, Ru→Rh and Ir→Cu. Fluid inclusions were measured on doubly polished sections using a LINKAM 600 heating and freezing stage (Institute of Mineralogy, University of Graz), cooled by liquid nitrogen with lower and upper limits of –196 and 600°C, respectively (Shepherd, 1981). Volatiles released by cracking of pure chromite samples were analysed by a quadrupole mass spectrometer (Balzers QMS 511) under dynamic pumping conditions at the Austrian Research Centre, Seibersdorf. The all-metal apparatus is evacuated by two turbo pumps in series and a catalysator baffled rotary pump. Pumping rate is reduced by a diaphragm aperture to 22 l/s (STP N2). Pressure during analysis varied between 1×10^{-8} and 1×10^{-5} mbar. To reduce sorption effects measurements have been carried out at ~100°C. The following gases have been calculated to be present using the computer program SGAP (Dobrozemsky, 1972): H_2O, H_2, CH_4, C_2H_6, C_3H_8, CO, CO_2, N_2, H_2S and SO_2. Artificial gas mixtures of known composition were used for calibration (Dobrozemsky, 1990).

CHROMITITES: PETROGRAPHY AND GEOCHEMISTRY

Petrography

Chromite orebodies of the Main Ore Field at Kempirsai belong to the concordant, deformed podiform type. The mantle is of HOT (Harzburgite–Ophiolite-Type; Nicolas & Prinzhofer, 1983) affinity. Orebodies have lens-like, vein-like, pipe-like or tabular shapes of highly variable size; tabular bodies dominate. The boundaries of the orebodies with enclosing dunite are either well defined or diffuse. Common irregular features include satellite stringers of chromite ore extending into the wallrock and dunite–serpentinite veins penetrating the orebodies. Many deposits consist of massive and disseminated ore in a dunitic matrix. Gradual contacts between massive ore and dunite over a metre-range are frequent. A typical contact shows gradation from fine-grained disseminated spinel in the dunite through fine-grained nodular and coarse-grained nodular, to massive coarse-grained chromite ore. Blocks (in the metre-size) of serpentinized dunite completely enclosed by chromitite are common and point to replacement of dunite by chromitite. Internal layering parallel to the foliation in the surrounding dunite is present in places. The orebodies are often terminated by east–west trending, crosscutting faults. The major ore types are as follows:

(1) Massive ores composed of 90–95 vol. % chromian spinel generally form the central part of the orebodies. Grain sizes of chromite range from 2 to 20 mm. The matrix is composed of serpentine minerals, chlorite, brucite, minor olivine and accessory alloys, sulphides and arsenides. Massive ores are usually considered as recrystallized ores; the gradual contacts to dunite, however, suggest that coarse-grained ore is a primary feature.

(2) Nodular ores consist of rounded, ovoid or almost angular, mostly elongated aggregates of chromian spinel (common axial ratios are 5:1) in a serpentinized matrix. Textures are usually matrix-supported. The sizes of the nodules vary between 0·5 and 10 cm in diameter. Nodules are internally massive and consist of interlocking anhedral spinel grains usually <1 mm in diameter. Rarely, silicate cores with subordinate spinel grains are present within nodules ('orbicular ore'; e.g. at Stepninsk; Fig. 1). Nodules deformed by pull-apart textures (Cassard *et al.*, 1981) are disintegrated into fine-grained disseminated ores.

(3) Disseminated ores either occur along the margins of massive orebodies or form small independent orebodies, especially in the northwestern part of the Kempirsai Massif (BAT ores). These show a banded texture defined by alternation of fine-grained (<1 mm grain size) disseminated chromian spinel and serpentinized olivine. In the MOF, disseminated ores reach grain sizes of >3 mm. Schlieren or taxitic types (possibly caused by ductile deformation) are common in lower stratigraphic levels. In dunite and pyroxenite dykes, so-called 'occluded' ore consists of serpentinized nodules of silicates within a matrix of fine-grained chromite.

In the most tectonized types, fine-grained cataclastites consisting of chromite clasts and matrix minerals are developed. Such cataclastic chromitites frequently carry uvarovite and dolomite in veinlets between chromite clasts. A minor, but highly unusual rock type in the Diamond Pearl open pit consists of veins and lenses composed of coarse, green amphibole, chlorite and chromite; such chromite carries abundant fluid inclusions (see below).

MOF chromites usually are fresh, and are chemically and optically unzoned. Extensive oxidation to ferritchromit has not taken place; 'ferritchromit' (Spangenberg, 1943) or ferrit-chromite (Evans & Frost, 1975) is defined as highly reflecting borders surrounding chromite in many serpentinized chromite deposits (e.g. Bliss & MacLean, 1975; Jan & Windley, 1990). In the upper parts of the orebodies that are more affected by supergene alteration, narrow rims of ferritchromit often surround homogeneous chromite grains.

Chromitites of the BAT-type at the Stepninsk and other localities are either massive or of a coarse nodular or orbicular variety with abundant, large inclusions of silicate material. The latter type shows extensive oxidation to ferritchromit along cracks and grain boundaries. Chromite rims often show a porphyroblastic texture with included acicular silicate phases.

Table 1: Representative electron microprobe analyses (wt % and cations calculated to 32 oxygen) of chromian spinel from ores of the Kempirsai Massif

Sample:	82-5	231-8	40L2	40L3	DP2	AZ2	DP6	93-13	93-16	93-24	93-24	93-34
Location:	Voskhod	Voskhod	40 Let	40 Let	Diam.P.	Diam.P.	Diam.P.	Diam.P.	Diam.P.	Stepninsk	Stepninsk	'117'
Texture:	Diss	Diss	Mass	Nod	Mass	Mass	Amp	Amp	Brecc	Core	Rim	Mass
SiO_2	0·03	0·01	0·10	0·06	0·01	0·00	0·08	0·06	0·07	0·08	0·17	0·07
TiO_2	0·23	0·14	0·15	0·11	0·18	0·18	0·02	0·10	0·26	0·29	0·22	0·44
Al_2O_3	10·06	8·06	8·32	8·94	8·54	9·13	11·48	12·21	9·93	30·86	24·64	21·34
Cr_2O_3	56·71	61·13	60·60	60·87	60·24	60·97	57·24	61·48	59·86	36·37	44·75	44·33
FeO_{total}	18·98	13·91	13·31	13·36	14·32	14·08	17·43	11·82	14·01	16·26	15·14	17·38
MnO	0·30	0·30	0·30	0·40	0·43	0·43	0·54	0·26	0·40	0·18	0·33	0·26
MgO	13·50	15·69	16·22	15·45	16·72	14·68	12·78	14·79	14·85	15·75	13·89	15·06
NiO	0·13	0·10	0·03	0·11	0·22	0·12	0·09	0·01	0·00	0·14	0·16	0·13
Total	99·94	99·34	99·03	99·30	100·66	99·59	99·66	100·73	99·38	99·93	99·30	99·01
Si	0·008	0·003	0·026	0·016	0·003	0·000	0·021	0·015	0·018	0·019	0·041	0·018
Ti	0·044	0·028	0·029	0·022	0·034	0·035	0·004	0·019	0·050	0·050	0·040	0·081
Al	3·052	2·444	2·517	2·706	2·535	2·770	3·491	3·624	3·004	8·495	7·074	6·165
Cr	11·540	12·432	12·296	12·362	11·998	12·411	11·675	12·243	12·150	6·716	8·618	8·591
Fe^{3+}	1·304	1·067	1·080	0·858	1·396	0·748	0·788	0·064	0·709	0·649	0·146	1·047
Fe^{2+}	2·781	1·925	1·776	2·012	1·621	2·283	2·972	2·426	2·299	2·526	2·938	2·516
Mn	0·066	0·066	0·066	0·087	0·092	0·094	0·118	0·055	0·087	0·036	0·068	0·054
Mg	5·179	6·016	6·204	5·916	6·278	5·634	4·914	5·552	5·682	5·483	5·043	5·503
Ni	0·027	0·021	0·006	0·023	0·045	0·025	0·019	0·002	0·000	0·026	0·032	0·026
Total	24·001	24·002	24·000	24·002	24·002	24·000	24·002	24·000	24·000	24·000	24·000	24·001
cr-no.	79	84	83	82	83	82	77	77	80	44	55	58
mg-no.	65	76	78	75	79	71	62	70	71	68	63	69
$Fe^{3+}/\Sigma R^{3+}$	8·2	6·7	6·8	5·4	8·8	4·7	4·9	0·4	4·5	4·1	0·9	6·6

Diam.P., Diamond Pearl mine; '117', see Fig. 1; Diss, disseminated chromitite; Mass, massive chromitite; Nod, nodular chromitite; Amp, amphibole–chromite rock; Brecc, brecciated chromitite; Core, rim, from zoned disseminated chromite; *cr*-no., 100Cr/(Cr + Al); *mg*-no., 100Mg/(Mg + Fe^{2+}); $Fe^{3+}/\Sigma R^{3+}$, 100 $Fe^{3+}/(Fe^{3+} + Al + Cr)$.

Chromite chemistry

Two distinctly different types of chrome spinel are present in ultramafic rocks of the Kempirsai massif: (1) The quantitatively dominant, and economically important spinel type is the low-Al, high-Cr spinel [*cr*-number, i.e. 100Cr/(Cr + Al), >78] of the Main Ore Field (MOF). It occurs in large (>100 Mt) ore bodies within harzburgitic and dunitic mantle tectonites. (2) High-Al, low-Cr spinel (*cr*-number 40–60) is present in small deposits of the Batamshinsk type in the Batamshinsk uplift and the Stepninsk area (northern and western part of the Kempirsai Massif).

More than 300 spinel analyses from the Kempirsai Massif (Pavlov & Grigoryeva, 1977; Melcher *et al.*, 1994; G. Simon, unpublished data, 1994; this work) are used to illustrate chemical variations between chromites from different parts of the massif (Fig. 2). Selected microprobe analyses of chrome spinel are presented in Table 1. The two groups of spinel compositions discussed here are further subdivided into six subgroups, characterized by different stratigraphic and lithologic settings. Data points belonging to such subgroups are plotted as fields in Fig. 2 for simplicity. Only outliers from statistically well-defined fields are plotted as single analyses.

Group (1), high-Cr, low-Al spinel is present in all orebodies of the MOF, in dunite wallrocks, and in amphibole–chromite vein rocks (MOF). Chrome spinels from MOF orebodies cover only a narrow range in the *mg*-number [100 Mg/(Mg + Fe^{2+})] vs *cr*-number (Fig. 2a) and Ti vs *cr*-number diagrams (Fig. 2c). $Fe^{3+}/\Sigma R^{3+}$ [100Fe^{3+}/(Fe^{3+} + Al + Cr)] and *mg*-number show well-defined positive trends (Fig. 2b). The *cr*-number (78–85) and *mg*-number (63–85) values are uniform in all orebodies (Fig. 2a), but Ti contents (Fig. 2c) and calculated $Fe^{3+}/\Sigma R^{3+}$ (Fig. 2b) slightly increase from orebodies in the southern to the northern part of the MOF. Averages

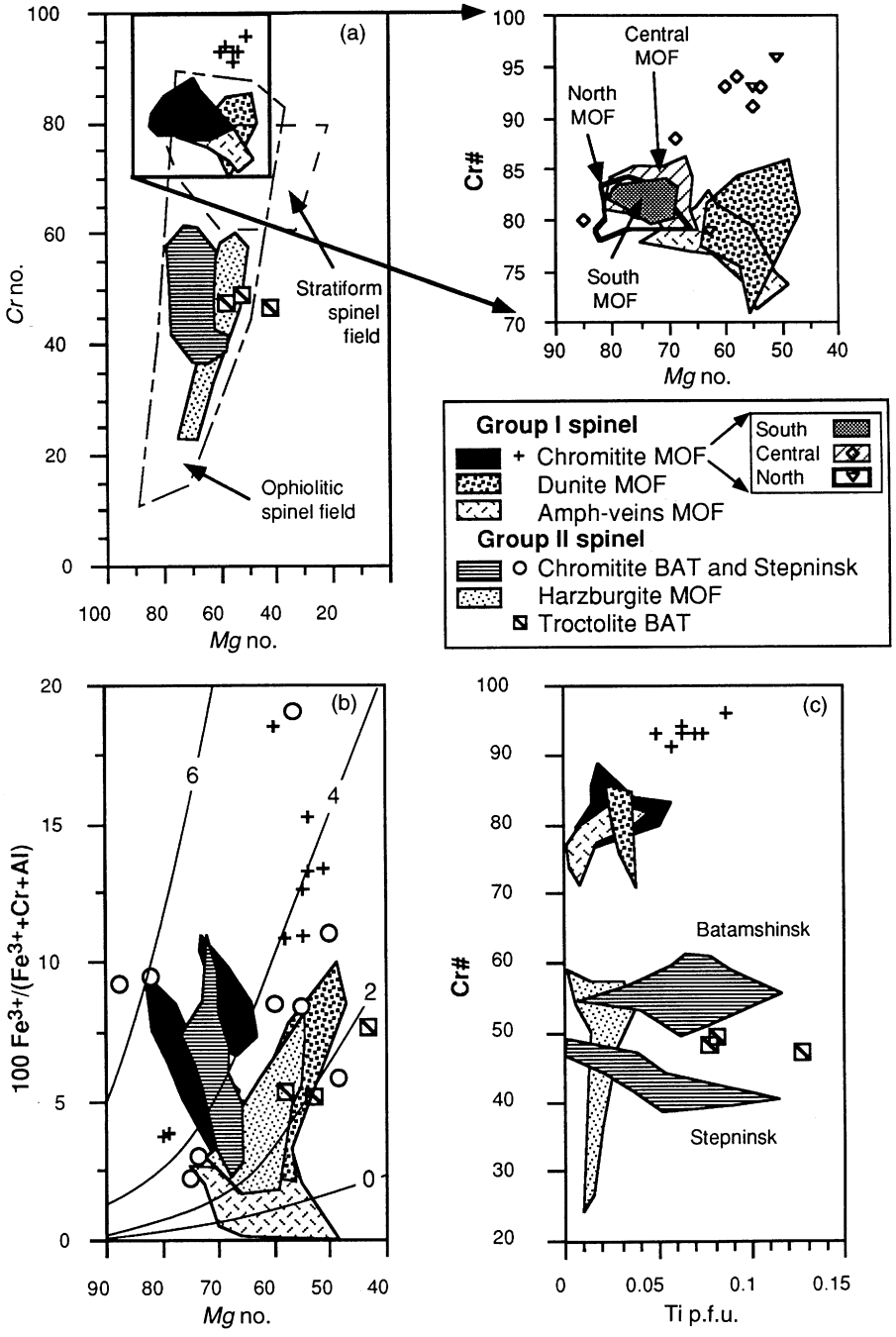

Fig. 2. Chemical composition of chrome spinel from the Kempirsai Massif. Two groups of spinel (high-Cr and low-Cr) are subdivided into six subgroups. Data are presented as fields. Outliers from statistically well-defined fields are plotted as single analyses. (a) Variation of *mg*-number [100 Mg/(Mg + Fe^{2+})] vs *cr*-number [100 Cr/(Cr + Al)]. Fields for chromites from stratiform and podiform deposits are shown (Dick & Bullen, 1984). The insert shows fields for MOF chromites discriminated according to their geographic position. (b) The *mg*-number vs 100 $Fe^{3+}/\Sigma R^{3+}$. Thin lines represent theoretical isobars for pure $(Mg,Fe)Cr_2O_4$ spinel. Numbers on the isobars are theoretically equal to $\log_{10} f(O_2)$ plus a constant (Irvine, 1965). (c) Ti p.f.u. (per formula unit) vs *cr*-number.

of $Fe^{3+}/\Sigma R^{3+}$ for the southern, central and northern orebodies are 6·1, 7·4 and 7·6, respectively. A group of spinel analyses from MOF orebodies, characterized by extremely high *cr*-number (>85, Fig. 2a), has elevated $Fe^{3+}/\Sigma R^{3+}$ and Ti, and lower *mg*-number than typical ore chromites. This is attributed to re-equilibration during serpentinization, increasing Cr, Ti and Fe^{3+}, and decreasing Al and Mg in primary chromite. Chrome spinel from amphibole–chromite veins is characterized by a spread in *cr*-number (71–83), scattering *mg*-number (48–75), and lower $Fe^{3+}/\Sigma R^{3+}$ (<5) than chrome spinel from massive, disseminated and nodular chromite ores. In dunitic envelopes, chrome spinel is depleted in Mg (*mg*-number 46–57) compared with massive ores, has constant Ti contents, and $Fe^{3+}/\Sigma R^{3+}$ slightly lower than ore chromites ($5{\cdot}5 \pm 3{\cdot}2$).

Harzburgite from the MOF, and chromitite and troctolite from the northern and western parts of the massif (BAT) belong to group (2), high-Al, low-Cr spinel. The *cr*-number values scatter widely in harzburgite (24–59) and BAT chromitite (38–60), but are nearly constant in troctolite (47–49). The *mg*-number values in troctolite are among the lowest (43–58), and Ti contents are the highest (up to 0·13 Ti p.f.u.) measured during this study. Accessory spinels in harzburgite and concordant dunite have low $Fe^{3+}/\Sigma R^{3+}$ and Ti contents. In the *cr*-number vs *mg*-number diagram (Fig. 2a) they follow a trend defined for abyssal peridotites, or Type I Alpine peridotites (Dick & Bullen, 1984). Batamshinsk-type chromitite is characterized by a wide range in *mg*-number (50–88) and Ti contents (up to 0·12 Ti p.f.u.). These chromites are compositionally zoned: rim compositions are enriched in Cr (*cr*-number up to 60), Fe^{2+} and Mn with respect to core compositions. Spinels from small orebodies in refractory harzburgite and dunite of the Tagashasai ore field (Fig. 1) are more chromian than those from lenses close to the crust–mantle transition at Stepnisnk.

MINERAL INCLUSIONS IN CHROMITE

Chrome spinel frequently carries solid inclusions of silicates, alloys, sulphides, sulpharsenides and arsenides. Many of these are considered as 'primary' on textural grounds, such as euhedral shapes within homogeneous, unaltered chrome spinel. Primary inclusions are located in areas of chromite that are free of fissures or cracks. Other inclusions are clearly 'secondary' with respect to chromite formation. Such inclusions may be euhedral, but are usually anhedral or subhedral and are frequently associated with cracks or serpentine-filled veinlets in chromite. The latter group most probably formed during serpentinization processes. The abundance of inclusions in chromite varies within the orebodies and also among different chromite types. Massive or highly brecciated chromites in the MOF carry fewer inclusions than nodular or disseminated varieties. Inclusions generally are distributed randomly in the spinel host, but in the coarse disseminated type, roughly zonal arrangements may be observed (Fig. 3a). Inclusions in BAT spinel are characteristically rounded (Fig. 3b), whereas in MOF chromite subhedral and euhedral shapes of negative crystals following spinel symmetry prevail. Mineral inclusions are subdivided into solitary types [silicate, platinum-group mineral (PGM), base metal sulphide or arsenide (BMM)] and into polyphase inclusions, with silicate–silicate, silicate–PGM and silicate–BMM being most prominent.

Silicate inclusions

Four groups of silicate inclusions are observed in chromitite of the Kempirsai massif:

(1) Anhydrous silicates such as olivine (Ol), clinopyroxene (Cpx) and orthopyroxene (Opx).

(2) Hydrous high-temperature silicates such as pargasitic hornblende (Am) and phlogopite (Ph).

(3) Hydrous low-temperature silicates such as chlorite (Chl), serpentine (Srp) and hydrogarnet (Grt).

(4) Ti- and Mn-rich silicates in BAT chromitite, accompanied by Ti- and Mn-rich oxides.

Groups (1)–(3) occur in the MOF, and groups (2)–(4) in BAT chromitite. Representative major element compositions of inclusion minerals in chromite are listed in Appendix A.

Olivine

Anhedral and euhedral olivine occurs as solitary grains, rarely within composite inclusions in MOF chromite. It is more abundant in footwall samples of the Voskhod orebody, but was detected also in the Diamond Pearl, Millionnoe and 40 Years of Kazakh SSR mines. Olivine is highly magnesian (*mg*-number 96·2–98·2) and contains high amounts of NiO (0·52–1·34 wt %) and Cr_2O_3 (0·7–1·3 wt %; Fig. 4a), but only low CaO (<0·06 wt %) and MnO (<0·1 wt %). For comparison, olivine in unaltered harzburgite has distinctly lower *mg*-number (89–91), NiO values typical for mantle rocks (0·2–0·4 wt %), and no detectable Cr_2O_3 contents. In strongly serpentinized dunitic envelopes of chromite orebodies, relict olivine has a composition similar to olivine in harzburgite, but with slightly elevated *mg*-number (92–93). Olivine compositions show positive correlations between Mg, Cr and Ni contents (Fig. 4a), and negative ones between Mg and Mn.

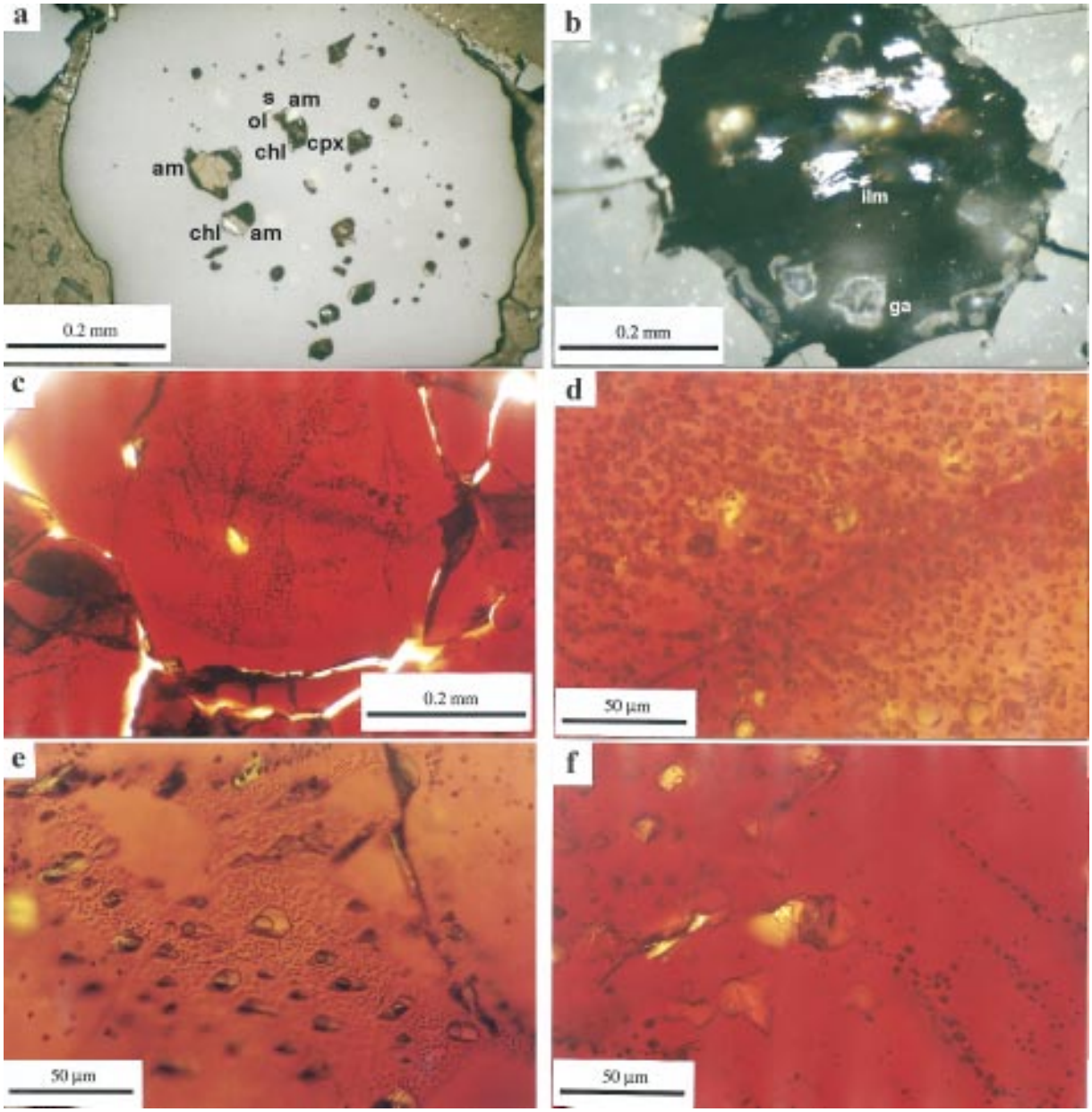

Fig. 3. Photomicrographs of inclusions in chromite. (a) Polyphase inclusions in disseminated chromite, Millionnoe (93-11); reflected light, oil immersion. (b) Polyphase inclusion in orbicular chromite, Stepninsk (93-24); reflected light, oil immersion. Dark phase is chlorite, light phase is chromite. (c) Fluid inclusions in chromite core surrounded by inclusion-free rim, Diamond Pearl (287-6); transmitted light. (d) Negative crystal-shaped two-phase (L + V) fluid inclusions occupy central part of chromite of Fig (c). (e) Chromite containing large and very small two-phase inclusions, Diamond Pearl (93-13). (f) Trails of small fluid inclusions and larger amphibole inclusions in chromite, Diamond Pearl (287/6). am, amphibole; ol, olivine; cpx, clinopyroxene; chl, chlorite; ga, hydrogarnet; ilm, ilmenite; s, copper sulphide + native copper.

Cr contents in inclusions are consistently high, independent of inclusion size. Thus, the contribution of Cr from chrome spinel from secondary fluorescence in such inclusions may not account for all of the Cr present in inclusion olivine. Elevated Cr^{2+} contents in olivine are only possible at very high temperatures or at very low oxygen fugacities (Li *et al.*, 1995). On the other hand, Cr^{3+} may substitute over a vacancy-coupled mechanism into the octahedral site in Mg_2SiO_4. This is described by the reaction (Lehmann, 1983)

$$Mg_2SiO_4 + 2FeCr_2O_4 = Cr_2SiO_4 + MgCr_2O_4 + MgFe_2O_4.$$

Maximum Cr^{3+} in olivine occurs at high silica activity and high activity of $MgCr_2O_4$ in coexisting spinel, but is independent of $f(O_2)$, and favoured by high temperature (Lehmann, 1983) and low pressure. Experimental evidence shows that at high temperatures (1200°C) and sufficiently high oxygen fugacities, nickel also diffuses quickly from chromite into olivine (Lehmann, 1983). This is controlled by a reaction such as

$$Fe_2SiO_4 + 2NiCr_2O_4 = Ni_2SiO_4 + 2FeCr_2O_4.$$

The exceptionally high contents of Ni in olivine inclusions (up to 1·34 wt %) are therefore regarded as an argument for relatively high-temperature re-equilibration processes of olivine with chromite.

Pyroxenes

Clinopyroxene inclusions in MOF chromite are relatively rare. In taxitic chromite from Millionnoe and Diamond Pearl, however, they are fairly common and are frequently associated with amphibole and olivine (Fig. 3a). Clinopyroxene is diopside ($En_{51-54}Fs_{0-2}Wo_{44-48}$; *mg*-number 95–98; Fig. 4b, Appendix A) and contains higher Na_2O (0·1–0·7 wt %) and Cr_2O_3 (0·9–1·5 wt %), but lower Al_2O_3 (0·4–1·8 wt %) contents than accessory clinopyroxene in harzburgite (*mg*-number 92–95, Na_2O <0·4 wt %, Cr_2O_3 0·3–0·5 wt %, Al_2O_3 1·7–1·8 wt %).

Rounded or anhedral inclusions of orthopyroxene in chrome spinel are almost pure enstatite (Fig. 4b; *mg*-number 97–98), with low contents of Al_2O_3 (<0·3 wt %), and high Cr_2O_3 (0·9–1·5 wt %). In contrast, orthopyroxene from harzburgite host rocks has *mg*-number 88–95, elevated Al_2O_3 (0·7–3·5 wt %) and CaO (0·13–1·20 wt %), and lower Cr_2O_3 (0·15–0·64 wt %) contents than inclusion enstatite.

Pyroxene compositions such as those observed from inclusions cannot have crystallized from a basaltic liquid (Johan, 1986). They may be explained by exchange reactions between Cr–Al spinel and Al-bearing pyroxene, with diffusion of Al from pyroxene into spinel during cooling.

Amphibole as inclusions in chromite

Amphibole is by far the most abundant inclusion phase in MOF chromite. It forms euhedral and anhedral, monomineralic (<5 up to 200 μm) and composite inclusions with other silicates (diopside, chlorite), PGM (frequently with laurite and Os–Ir alloy), or base metal-rich minerals (BMM). Amphiboles are generally highly magnesian [*mg*-number ranges from 94 to 98 (Fig. 4d)], enriched in Cr_2O_3 (up to 4·0 wt %) and Na_2O (up to 3·5 wt %), and low in TiO_2 (<0·65 wt %) and K_2O (<0·28 wt %). Chlorine and fluorine contents in amphibole invariably are below the detection limit of the electron microprobe. Compositional variability of amphibole in ultramafic rocks of Kempirsai is expressed in diagrams of Al/(Al + Si) vs Na/(Na + Ca) and *mg*-number vs Si p.f.u. (Fig. 4c and d). Edenitic to pargasitic hornblende is most common, and a well-defined trend exists toward tremolite compositions. Amphibole inclusions in MOF chromite are slightly more magnesian than in BAT spinel, but considerably more magnesian than accessory amphibole in harzburgite host rocks. Small amphibole inclusions in BAT-type Al–Cr spinel at the Stepninsk locality carry considerably higher Ti and Al, and lower Si than MOF amphiboles; their Ni contents are on average somewhat higher (Appendix A).

Amphibole in veins

Although this section summarizes silicate inclusions in chromite, the following observations are highly relevant to the discussion. Coarse (up to 4 cm), dark green amphibole also occurs as matrix mineral to chromite in vein- and lens-like rocks at the Diamond Pearl mine; in such veins it is replaced by chromian clinochlore that exsolves rutile. Coarse amphibole has numerous, occasionally amoeboidal chromite inclusions. Larger chromite grains forming aggregates in an amphibole matrix frequently contain solid and fluid inclusions (see below). Vein-type amphibole covers a large range of compositions from tremolitic hornblende to pargasite. It is more variable in *mg*-number than inclusion amphibole. Oxygen and hydrogen isotope analyses performed on fractions of vein amphibole plot within the range of high-temperature mantle amphibole: $\delta^{18}O$ ranges from 6·0 to 6·7‰, and δD from –51 to –59‰ (Melcher *et al.*, 1997).

Sodium phlogopite

Inclusions of mica are rare in MOF chromite. Na-phlogopite was identified in samples from the Diamond Pearl mine as minute grains in vein-type chromite hosted by amphibole, and in massive chromitite in contact with Ni sulphide. It has high Na_2O (4·1–4·4 wt %), Cr_2O_3 (2·0–3·56 wt %) and NiO (0·5–0·7 wt %) contents, whereas K_2O (<0·8 wt %) and TiO_2 (<0·32 wt %) are low. A K–Ca-bearing aluminosilicate of unknown composition was observed as part of a three-phase composite inclusion in BAT spinel together with apatite and Ni sulphide.

Garnet

Calcium- and Cr-rich garnets are present in three textural associations with chromite (Fig. 5). In all these associations garnets are considered as secondary minerals that formed during relatively low-temperature processes. Garnet occurs in the following forms:

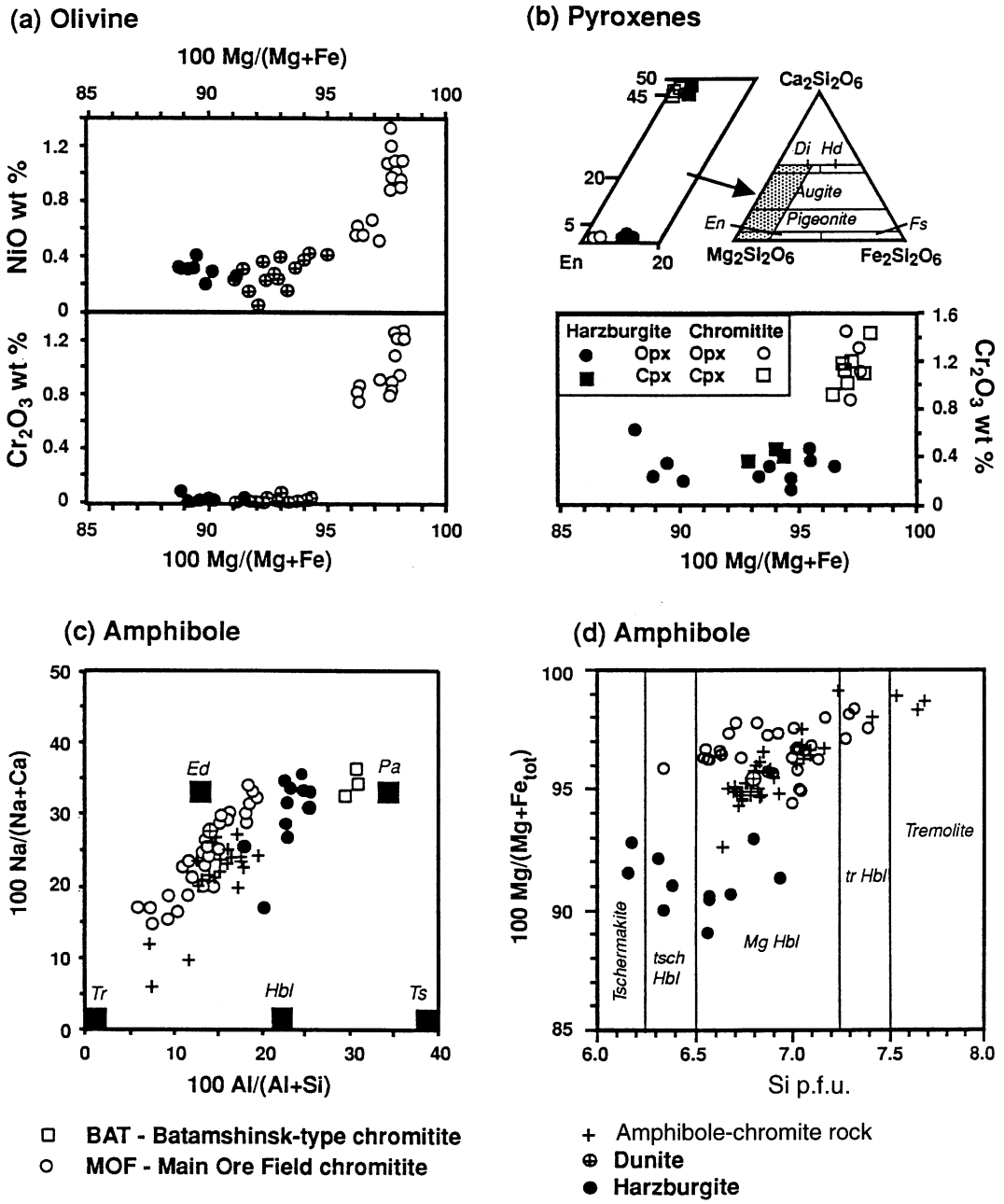

Fig. 4. Compositional variations of silicate phases included in MOF and BAT chromite, compared with harzburgite and dunite. (a) 100Mg/(Mg + Fe) vs wt % Cr_2O_3 and NiO, respectively, for olivine. (b) Pyroxene quadrilateral, and 100Mg/(Mg + Fe) vs wt % Cr_2O_3 in pyroxene. End members: En, enstatite; Di, diopside; Fs, ferrosilite; Hd, hedenbergite. (Note that the legend for pyroxenes is different from that for the other diagrams.) (c) 100Al/(Al + Si) vs 100Na/(Na + Ca) for amphiboles. End members: Ed, edenite; Hbl, hornblende, Pa, pargasite, Tr, tremolite, Ts, tschermakite. (d) Si p.f.u. vs 100Mg/(Mg + Fe_{tot}) for amphiboles.

(1) Small (20–30 μm), euhedral uvarovite ($Uv_{68}Grs_{12}And_{18}Prp_2$) occurs as inclusions in chromite of the MOF. It is associated with amphibole, chlorite and Ni sulphide.

(2) In narrow veinlets in highly brecciated chromite of the MOF, euhedral uvarovite-rich garnet ($Uv_{77-88}Grs_{1-4}And_{7-22}$) is present coexisting with dolomite ($Cc_{50}Mg_{50}$).

(3) Calcian Al–Ti–Cr garnets ($Uv_{8-38}Grs_{27-64}And_{18-32}$) are present as small anhedral grains or lamellar intergrowths with chlorite interstitial to, and in composite inclusions within, BAT-type spinel at Stepninsk (Fig. 3b).

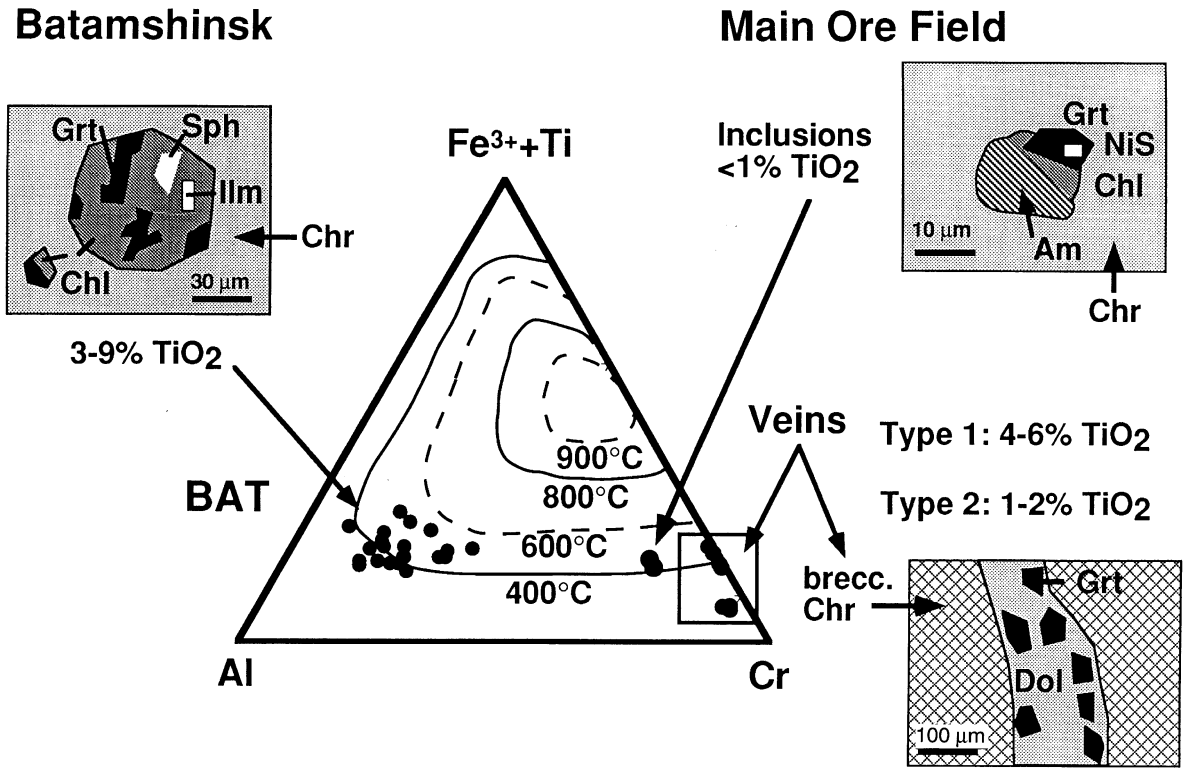

Fig. 5. Triangular diagram of garnet and hydrogarnet compositions in the system grossular ($Ca_3Al_2[SiO_4]_3$)–uvarovite ($Ca_3Cr_2[SiO_4]_3$)–andradite ($Ca_3(Fe,Ti_2)[SiO_4]_3$). Lines are calculated stability limits of ugrandite solid solution depending on temperature (after Ganguly, 1976). Three textural types of garnet are illustrated in sketches. Am, amphibole; Chl, chlorite; Chr, chromite; Dol, dolomite; Grt, garnet; Ilm, ilmenite; Sph, sphene.

Types (2) and (3) carry appreciable hydrogarnet components.

All garnets analysed are dominated by Ca in their X-sites. The contents of Fe^{2+}, Mn and Mg are generally very low (Appendix A). The Y-sites contain variable amounts of Cr, Al, Fe^{3+} and Ti. With the exception of type (1), garnets contain unusually high Ti contents (up to 9 wt % TiO_2). In assemblages (2) and (3), the tetrahedral sites are silica deficient, and analytical totals range from 96 wt % [assemblage (3)] to 99 wt % [assemblage (2)]. This suggests the presence of hydroxyl groups; H_2O contents recalculated from microprobe analyses range from 1·5 to 4·5 wt %, identical to 0·3–1·2 mol % H_2O p.f.u. The minerals thus belong to the hydro-ugrandite series (Deer *et al.*, 1982). Natural garnets show continuous solid solution between grossular and both andradite and uvarovite, but only limited substitution between Fe^{3+} and Cr^{3+}. On a ternary diagram of andradite (Fe^{3+} + Ti), grossular and uvarovite components (Fig. 5), the available analyses, calculated as anhydrous garnets, plot close to the 400°C or 500°C isotherm (Ganguly, 1976).

Ti- and Mn-rich phases (ilmenite, sphene, Ca–Ti oxide)

Chlorite inclusions within spinel of the BAT frequently carry lamellar or anhedral inclusions of manganoan ilmenite, sphene and a Ca–Ti oxide (Fig. 5). MnO contents of up to 17 wt % are detected in ilmenite in addition to traces of Cr_2O_3 (0·7–0·8 wt %), MgO (up to 0·2 wt %) and CaO (up to 0·6 wt %; Appendix A). Manganoan ilmenite also forms skeletal aggregates in interstices between spinel grains. In this position it often coexists with Cr-enriched spinel rims. Matrix ilmenite has lower MnO (10–13 wt %) than inclusion ilmenite.

Inclusion ilmenite occasionally contains triangular-shaped inclusions of a Ca–Ti oxide phase (Appendix A). Calculated formulae are not compatible with perovskite ($CaTiO_3$), loveringite ($CaTi_{21}O_{38}$) or other more common large ion lithophile element (LILE)-enriched Ti oxides (Haggerty, 1991). A formula of $(Ca_{0·80}Mg_{0·08}Mn_{0·04})_{0·92}(Ti_{2·86}Al_{0·04}Cr_{0·10}Fe^{3+}_{0·05})_{2·95}O_7$ resembles zirkelite (XY_3O_7, with X = Ca, Ce, Y, Fe, and Y = Ti, Zr, Th). Sphene also forms inclusions in chlorite within BAT spinel. It contains minor amounts of the oxides of Fe (0·5 wt %), Al (1·4–1·7 wt %), Cr (1·1–1·4 wt %), V (0·6 wt %), Mg (0·1–0·4 wt %) and Ni (0·03–0·06 wt %).

Ti- and Mn-rich minerals are rarely reported from ophiolitic–podiform chromitites. Perovskite and loveringite, however, are common constituents of mineral inclusions in chromite-rich parts of mafic–ultramafic intrusions (e.g. Lorand & Cottin, 1987; Johan, 1995). As

all the above-mentioned Ti- and Mn-rich minerals are only present in association with chlorite in BAT chromite, they are considered as secondary inclusions, although Ca–Ti oxide may represent a relict high-temperature phase.

Chlorite and serpentine

Cr- and Mg-rich clinochlore ('kämmererite') is frequent as (1) inclusions in MOF and BAT chromite, (2) a component of vein-type amphibole–chlorite–chromite rock (MOF) and (3) a matrix mineral in both settings. Chlorite compositions cover a wide range of silica contents (Si = 5·1–6·9 atoms p.f.u.). Composite inclusions of chlorite with amphibole, garnet and Ni sulphides are common in MOF chromite. Texturally, clinochlore is a secondary mineral in MOF chromitite.

Chlorite inclusions in BAT-type Al–Cr spinel at Stepninsk are 50–200 μm in diameter and frequently consist of a porous-looking, inhomogeneous core and a clear rim with abundant inclusions of garnet, ilmenite, sphene, and Ni sulphides and arsenides. Core compositions are enriched in Fe and Cr, and depleted in Al, Mg and Ni compared with rims. Matrix chlorite in BAT ores resembles compositions of inclusion rims. Compared with MOF chlorite, BAT chlorite has higher Al and Fe, and lower Mg and Si contents (Appendix A).

Serpentine and talc-chlorite are abundant in all chromite types of the MOF, except vein-type amphibole–chromite rock, either as inclusions or as a matrix mineral surrounding chromite. Serpentine inclusions are chemically distinct from matrix serpentine in that they contain elevated Al, Cr, Ti and Si, and lower Mg, Ni and Cl contents (Appendix A). The *mg*-number values are slightly lower (95–97 compared with 97–98 in the matrix). According to powder X-ray diffraction analyses on cleaned material, matrix serpentine is dominated by 1M lizardite. 1M lizardite and brucite predominate in the matrix of chromitite, typically forming pseudomorphic mesh textures after olivine (Wicks & Whittaker, 1977). Lizardite carries detectable chlorine in the 0·1 wt % range. Fine-grained, chlorine-bearing lizardite is frequently observed as an early stage in the transformation of olivine to serpentine (Miura *et al.*, 1981), and chlorine is attributed to hydrothermal solutions. The observation of a discrete Fe chloride phase, hibbingite, γ-$Fe_2(OH)_3Cl$, in serpentinized olivine-rich rocks (Saini-Eidukat *et al.*, 1994) underlines the importance of chlorine during serpentinization. Its potential significance for base and precious metal transport has already been stressed by Rucklidge & Patterson (1977).

Platinum-group mineral inclusions

Inclusions of platinum-group minerals (PGM) of <1 μm up to 20 μm size were identified in about 30% of polished sections investigated from chromitite bodies of the MOF. They are relatively frequent in massive chromitite and in coarse-disseminated or taxitic (schlieren) type chromitite. Nodular varieties, strongly brecciated chromitite, vein-type chromitite, and disseminated chromite in dunite are usually poor in PGM. In BAT chromitites, only a few grains of Os–Ir alloy and laurite were observed. Two textural groups of PGM can be distinguished in Kempirsai chromitite: (1) euhedral and anhedral solitary and composite PGM in undeformed chromitite, and (2) composite PGM inclusions forming trails in both undeformed and deformed chromite which are associated with serpentine, chlorite and base metal minerals (BMM) (Fig. 6). Within both textural groups, four chemical groups of PGM can be distinguished (Table 2) (Melcher *et al.*, 1995). Representative analyses are given in Appendix B.

Group (1) inclusions are considered as primary inclusions. They occur both as monophase or composite (polyphase) grains in undeformed chromite. Sulphides of the laurite–erlichmanite solid solution series are the most common monophase inclusions, followed by Os–Ir alloys and Ni–Cu–Ir–Os sulphides. Polyphase inclusions frequently consist of a silicate (usually amphibole, in about 50% of polyphase inclusions), and/or laurite (RuS_2), erlichmanite (OsS_2), Os–Ir alloy and Ni–Cu–Ir–Os sulphide.

Group (2) inclusions are texturally closely associated with cracks and with serpentine- or chlorite-filled veins in chromite, and are also found in the serpentine matrix surrounding chromite. Such inclusions frequently form trails in brecciated chromite. They are generally anhedral and composite (up to six phases), and are associated with sulphides and arsenides of Ni and Fe. The paragenesis of PGM includes all of the group (1) minerals except Os–Ir alloys and Ir–Rh sulphides; in addition, complex alloys combining PGE and base metals occur, as well as Ir–Os–Ru sulpharsenides and arsenides.

Os–Ir–Ru alloys

Osmium–iridium alloys, with up to 14 at. % Ru, are restricted to group (1) inclusions. They make up about 16% of the monophase, and 24% of all PGM detected in composite inclusions. Lamellar crystals of cubic iridium ($Ir_{60-100}Os_{0-40}$) and lath-shaped hexagonal osmium ($Os_{42-100}Ir_{0-58}$) with several at. % Ru are associated with laurite–erlichmanite ± amphibole, or with Ni–Ir sulphide ± amphibole. Intermediate rutheniridosmine (after Harris & Cabri, 1991) with up to 22 at. % Ru was observed in a few cases (Fig. 7a).

PGE–BM alloys

Some alloys present in massive Kempirsai chromitite combine variable amounts of Ir, Os, Ru, Pt, Fe, Ni and Cu (Fig. 7a and d). They often occur in association with

Table 2: Ranges of chemical compositions (wt %) of platinum-group minerals found in the Kempirsai Massif; the distinction of groups (1) and (2) is adhered to in the text

Approx. composition	Mineral name	Abundance	Group	Ir	Os	Ru	Rh	Pt	Ni	Cu	Fe	As	S
Alloys													
Os–Ir–(Ru)	Iridium, osmium	xxx	1	0–97	0–96	<11	<1	<6	<1·2	<1·1	<3·5		
(Os,Ru)(Cu,Fe)	Unknown	x	1	7·0–9·0	41–49	15–23	<0·5		<0·5	22–30	4·0–5·0		
$Ir(Ni,Fe)_{1·5–5·0}$	Unknown	x	1	31–64	<4	<2	<0·1		24–52	<6	<4		
$(Ir,Pt)_7Fe$	Unknown	o	?	83	1·3			10			3·5		
Sulphides													
RuS_2–OsS_2	Laurite, erlichmanite	xxx	1,2	1·7–27·9	3·0–54·3	3·1–49·7	<8·6		<1·3	<2·6	<3·9	<1·4	22–39
$(Ir,Rh)S_2$	Unknown	x	1	62–67		<0·2	6·0–8·7		<0·7	<0·7	<0·8		24–27
$(Ir,Rh)_2S_3$	Kashinite	x	1										
PGE–BM–S	Unknown)	xxx	1,2	5·4–61·1	<44	<4·8	<5·5		0·1–21·1	0·5–13·6	0·2–7·3	<1·5	13–28
Sulpharsenides													
(Ir,Ru,Os)AsS	Ir(Os-,Ru-)arsite	xx	2	2–60	1–30	0–29	<8	<1	<1·7	<1·2	<0·1	21–29	7–13
$(Ni,Ir)_2AsS$	Unknown	o	2	1·6	4·3	28·5	3·4		36		1·4	28	13
$(Ir,Ni)_2AsS_2$	Unknown	o	2	31	3·9	0·3	0·3		9·4	0·4	1·7	15	11
$Ni_{0·8}Ir_{1·6}AsS_{0·4}$	Unknown	o	2	50–61	<0·5	—	<0·8		2	1	6–8	12–14	2–3
$(Ir,Ni)As_{0·6}S_{0·25}$	Unknown	o	2	60–61	<0·5	—	1·4–1·7		3	<1	7–8	19–20	2–3
$(Ir,Os)_2(S,As)_3$	Unknown	o	2	59	14·2	1·3	—		0·9	0·8	1·3	6	17
Arsenides													
$OsAs_2$	Omeiite	x	2	3	40–42	7	0·1		0·1	0·1		47	
(Ru,Ni)As	Ruthenarsenite	o	2	5	16	31	0·5		6·1		1·4	37	
$(Ir,Os)_2As$	Unknown	o	2	47–51	31	<0·3	<0·1		<0·3			14–17	
$(Ni,Os)_2As$	Unknown	o	2	1·3	27	6·8	1·2		32	—	0·7	30	1·4
$(Ni,Ir)_3As$	Unknown	x	2	8–25	<2	<0·5	<0·2		46–57		<1·9	24–32	<0·7
RhNiAs	Unknown	o	2				43		24			32	

Abundances: xxx, very frequent; xx, frequent; x, moderately abundant; o, rare.
PGE–BM–S: $(Ir,Os,Ru,Rh,Ni,Cu,Fe)_{1-x}S$.

euhedral sulphide inclusions. Some of these alloys have porous surfaces, and carry inclusions (or relics) of laurite, erlichmanite and Ir–Os alloys. Cu–Os alloys form polyphase inclusions with Ir–Cu sulphide, Ir-sulpharsenide and amphibole. Chemical compositions of composite alloys are variable; PGE:BM ratios approach 1:1 in (Os, Ru)(Cu,Fe), and 1:1·5, 1:3 and 1:5 in Ir–(Ni,Fe) alloys. One grain of (Ir,Pt,Fe) having an (Ir + Pt)/Fe ratio close to seven is reported.

PGE sulphides

Minerals of the laurite–erlichmanite solid solution series are the most frequent PGM observed in chromitites of the Main Ore Field. They form 68% of all monophase inclusions and 42% of the PGM detected in composite inclusions. Laurite–erlichmanite varies chemically between $Ru_{0·94}Os_{0·04}Ir_{0·02}S_2$ and $Ru_{0·14}Os_{0·74}Ir_{0·12}S_2$. Iridium contents are as high as 27·9 wt % (11·5 at. %) in some solid solutions that are part of composite inclusions; generally, Ir is higher in Os-rich minerals (Fig. 7b). Rhodium contents are usually low (<2 wt %), but occasionally as high as 8·6 wt % Rh (6·4 at. %). Arsenic is present only in small amounts (up to 1·4 wt %). Laurite is restricted to group (1) inclusions and forms euhedral and anhedral grains of 2–20 μm size. Euhedral laurite often is solitary and Os poor, but composite inclusions with anhedral amphibole and Ir–Ni sulphide have been observed. Anhedral laurite occurs in both monomineralic

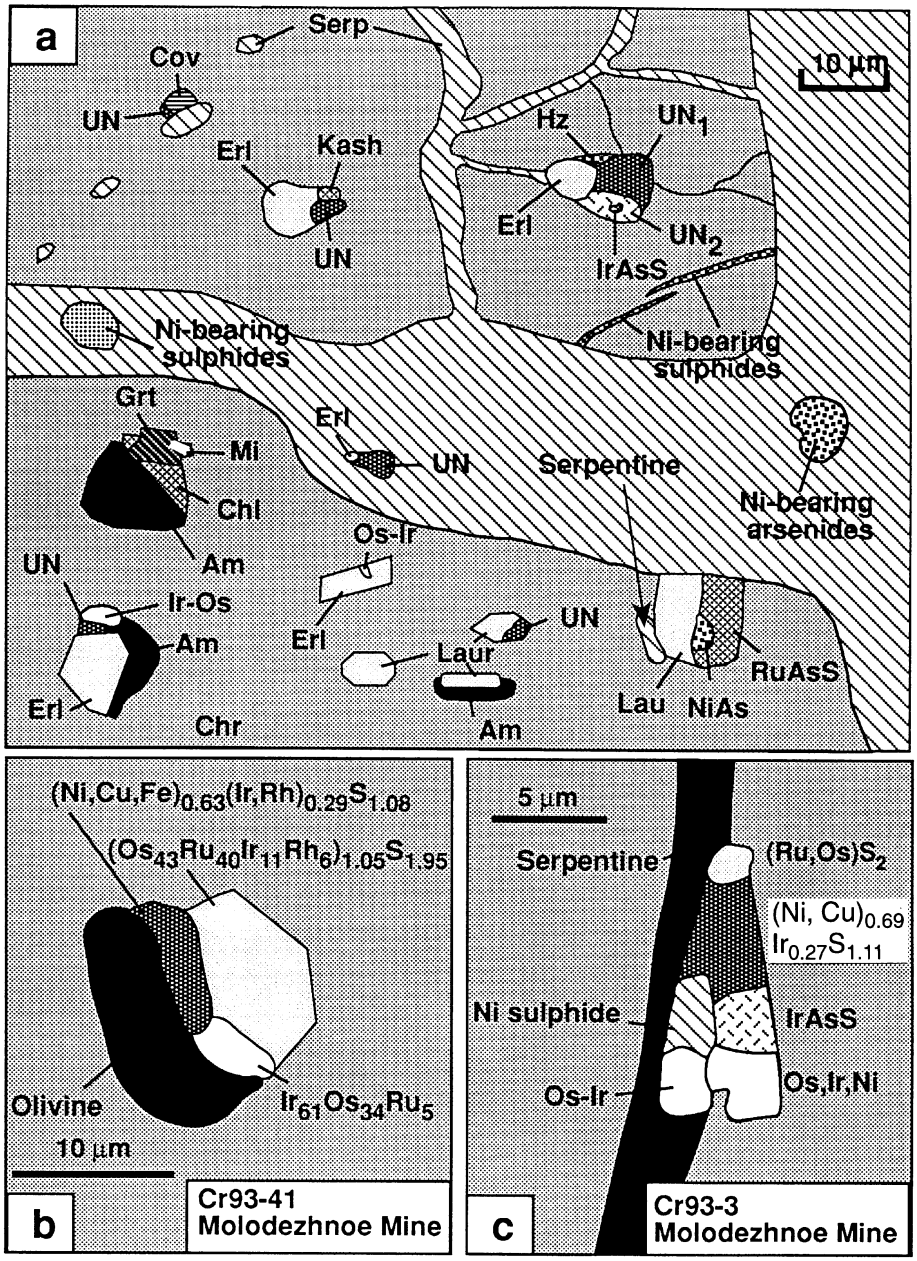

Fig. 6. Textural attributes of platinum-group mineral, base metal sulphide, and silicate inclusions in chromitite of the Main Ore Field, Kempirsai Massif. (a) Schematic sketch showing typical primary group (1) and secondary group (2) inclusions. Am, amphibole; Chl, chlorite; Chr, chromite; Cov, covellite; Erl, erlichmanite; Grt, garnet; Hz, heazlewoodite; IrAsS, irarsite; Os–Ir, Os–Ir alloy; Kash, kashinite; Lau, laurite; Mi, millerite; NiAs, Ni arsenide; RuAsS, ruarsite; Serp, serpentine; UN, unknown (Ir, Os, Rh, Ni, Cu, Fe) sulphides. (b) Polyphase group (1) inclusion in chromite, containing olivine, Os–Ir alloy, laurite and (Ni, Cu, Fe, Ir, Rh) sulphide. (c) Polyphase group (2) inclusion in a serpentine veinlet in chromite, containing laurite, (Ni, Cu, Fe, Ir, Rh) sulphide, irarsite, Ni sulphide and two alloys.

and composite inclusions. Erlichmanite is frequent and only rarely exhibits euhedral crystal shape. It is common as an anhedral mineral in inclusions of groups (1) and (2). Laurite is also present as large, zoned grains within BAT spinel, with a core enriched in Os (Melcher *et al.*, 1994).

Few grains of Ir–Rh sulphides <7 μm in size occur in composite type (1) inclusions, or as single inclusions. They are kashinite–bowieite, $(Ir,Rh)_2S_3$, with Ir:Rh = 1:1, and unnamed $(Ir,Rh)S_2$. The latter phase has constantly high Ir values (Ir:Rh = 4:1) and may be identical with isotropic IrS_2 [UN 1974-5 of Cabri (1981)].

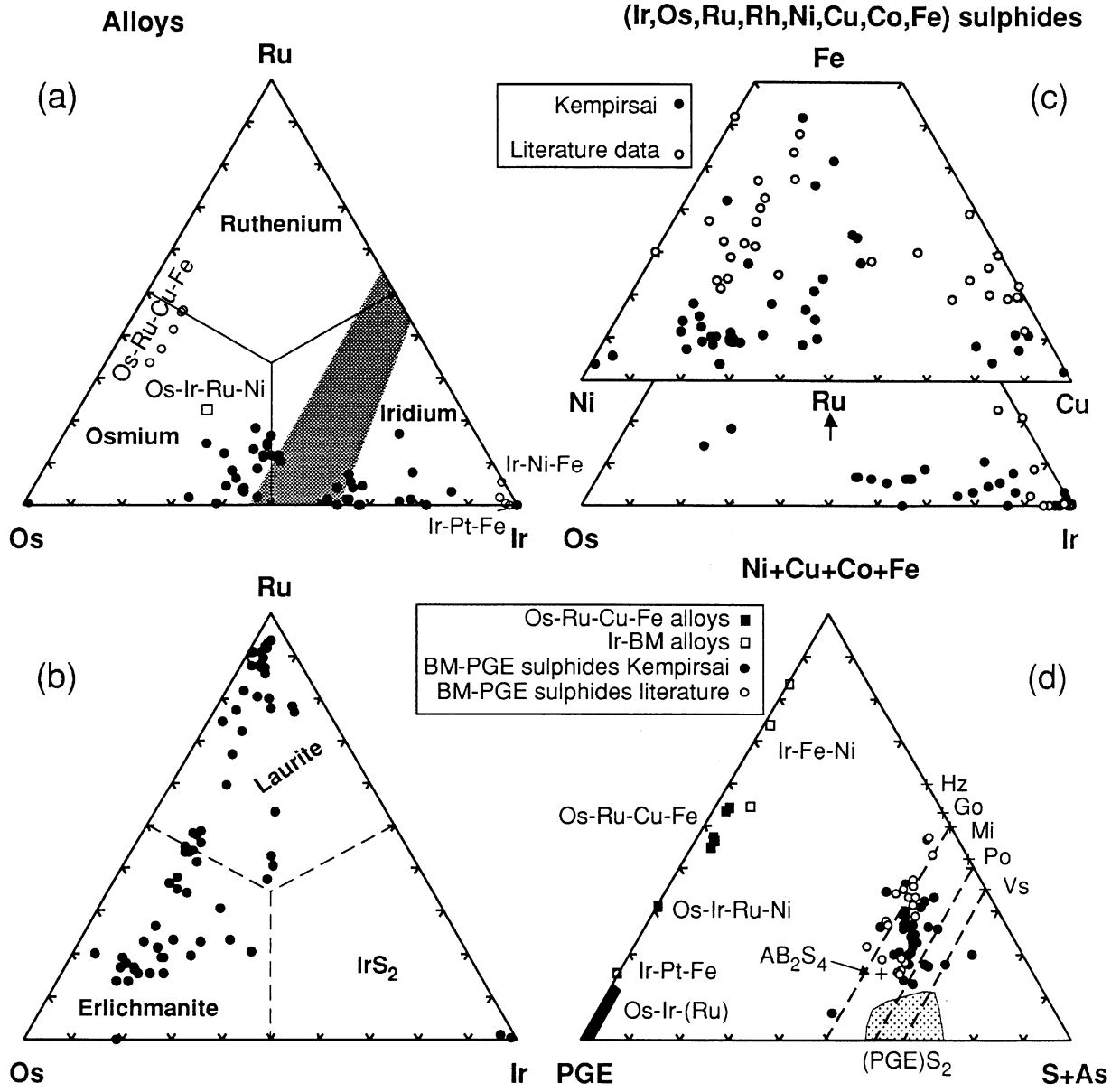

Fig. 7. Triangular diagrams illustrating compositions of platinum-group minerals of Kempirsai chromitites. (a) Ru–Os–Ir diagram for alloys. Nomenclature of PGE alloys according to Harris & Cabri (1991). (b) Ru–Os–Ir diagram for PGE disulphides. (c) Ru–Os–Ir and Fe–Ni–Cu diagrams for complex (Ir, Os, Ru, Rh, Ni, Cu, Co, Fe) mono-sulphides. Data from Yu *et al.* (1974), Stockman & Hlava (1984), Augé (1988), Ferrario & Garuti (1990), McElduff & Stumpfl (1991) and Torres-Ruiz *et al.* (1996) are shown for comparison. (d) Base metal–PGE–(S + As) diagram for PGE-bearing alloys and sulphides. On the BM–(S + As) join, ideal compositions of sulphides in the Ni–S system are given for comparison. Hz, heazlewoodite; Go, godlevskite; Mi, millerite; Po, polydymite; Vs, vaesite. The composition of PGE-rich thiospinel AB_2S_4 (e.g. cuproiridsite) is also indicated.

Complex (Ir, Os, Rh, Ni, Cu, Fe) sulphides

BM–PGE sulphides are frequent in MOF chromitites (Melcher *et al.*, 1994, 1995). They usually are anhedral and part of composite inclusions (with laurite–erlichmanite, Ir–Os alloy, silicates) in both primary and secondary PGM-bearing inclusions (Fig. 6). BM–PGE sulphides make up ~16% of the monophase inclusions, and 26% of the inclusion inventory in polyphase inclusions. The minerals are brownish grey in reflected light and have relatively lower spectral reflectance (Y% ~33%) than laurite (42%).

There is considerable chemical variation in terms of Ni–Cu–Co and Ir–Os–Rh–Ru (Fig. 7c and d) within this mineral group, with Ni and Ir usually dominating

(Appendix B). Fe contents are low, in contrast to other reported compositions, but there seems to be extensive substitution of Ni by Cu (Fig. 7c). Formulae are in the range $\Sigma BM_{0\cdot12-0\cdot65}\Sigma PGE_{0\cdot21-0\cdot92}S_{0\cdot90-1\cdot40}$, with BM = Ni + Cu + Co + Fe and PGE = Ir + Os + Ru + Rh. BM–PGE ratios range from 0·1 to 2·0, but are more frequently >1; (ΣBM + ΣPGE)/S shows smaller variations from 0·62 to 1·23. In a diagram of BM, PGE and S (Fig. 7d), most data plot on a linear trend between monosulphide [(BM,PGE)S] and hypothetical [$(BM,PGE)_3S_4$] solid solutions.

Most minerals are close to $(BM,PGE)_{1-x}S$, with x = 0·0–0·4. Among PGMs, such compositions are reported from tetragonal vysotskite, (Pd,Ni)S and cubic 'xingzhongite', (Ir,Cu,Rh)S (Cabri, 1981), redefined as (Pb,Cu,Fe)$(Ir,Pt,Rh)_2S_4$ (Anthony *et al.*, 1990). A few analyses resemble a thiospinel formula, AB_2S_4, such as cuproiridsite, $CuIr_2S_4$. Chemically variable PGE-rich BM sulphides of (BM,PGE)S and $(BM)_2(PGE)S_3$ composition have been reported from a few chromite occurrences, namely Finero, Italy and Ojén, Spain (Ferrario & Garuti, 1990; Garuti *et al.*, 1995; Torres-Ruiz *et al.*, 1996), New Caledonia (Augé, 1988), and Troodos, Cyprus (McElduff & Stumpfl, 1990).

Because of the extremely variable composition of complex (Ir, Os, Rh, Ni, Cu, Fe) sulphides at Kempirsai, we assume the presence of a high-temperature PGE–BM solid solution, probably of the millerite-type, $(Ni,Cu,Co,Fe,Ir,Os,Rh)_{1-x}S$. Above 379 ± 3°C, trigonal, stoichiometric low-temperature millerite, NiS, transforms to hexagonal high-millerite, $Ni_{1-x}S$, having a NiAs structure (Kullerud & Yund, 1962). The NiAs structure type exhibits an extensive solid solution with PGE.

PGE sulpharsenides

PGE-bearing sulpharsenides of the group irarsite (IrAsS)–osarsite (OsAsS)–ruarsite (RuAsS) are generally associated with serpentine veinlets and form composite inclusions of type (2), with PGE sulphides, alloys and arsenosulphides (Fig. 6). PGE arsenides and sulpharsenides form only 5% of all PGM found in composite inclusions, and never occur as single phases.

Most members of the irarsite series are dominated by Ir, but there is considerable substitution of Ru, Os and Rh. A few arsenic- and sulphur-bearing inclusions contain elevated base metal contents. Calculated formulae are $(Ni,Ir,Os)_2AsS_2$ and $(Ni,Ru,Os,Rh)_2AsS$, and may be new minerals. The former corresponds to a formula similar to daomanite, $(Cu,Pt)_2AsS_2$. Both are, however, minute grains (<5 μm) intimately intergrown with other PGE and BM phases, and microprobe analyses alone are thus not sufficient to characterize them as new minerals.

In addition to BM–PGE sulphide, there are few grains of (Ni, Cu, Fe, Ir, Rh) sulpharsenide with As/S approaching 2·5. These form polyphase inclusions with erlichmanite, irarsite, heazlewoodite and (Ir, Rh, Cu, Co, Ni, Fe) arsenosulphide. Rare (Ir, Os, Ru) arsenosulphide occurs in association with erlichmanite and Ni–Ir sulphide.

PGE and PGE–BM arsenides

Arsenides are rare and, because of the extremely small grain size, difficult to analyse. Omeiite, $(Os,Ru,Ir)As_2$, ruthenarsenite (Ru,Ni)As, and minerals approximating $(Ir,Os)_2As$, $(Ni,Os)_2As$ and $(Ni,Ir)_3As$ (Ir-bearing dienerite) were observed (Appendix B). Such arsenides form anhedral crystals in massive chromitite, and are associated with complex sulpharsenides ± amphiboles. They frequently replace Ir–Os alloys. Occasionally, ruthenarsenite is surrounded by ruarsite. There is also one monomineralic anhedral grain of NiRhAs, 7 μm in size.

Base metal minerals (BMM)

Base metal-rich alloys, sulphides and arsenides with <2 wt % PGE occur either as inclusions within chromite or, far more abundant, in veinlets in chromite and in the silicate matrix. The total amount of PGE-poor base metal mineral inclusions in chromites is many times smaller than the amount of PGM. Furthermore, 'primary' PGM are only rarely associated with BMM. This indicates that PGM and BMM did not crystallize together in most cases. Table 3 summarizes the BM-rich minerals detected as inclusions in chromite, and occurring in cracks of chromite or interstitial in the matrix. Some representative analyses of Ni sulphides and Ni arsenides are presented in Appendix B.

Base metal minerals as inclusions in chromite

Base metal mineral inclusions in chromite are generally anhedral and 5–20 μm in size. They occur in the following forms: (1) as single discrete grains, (2) as inclusion trails, or (3) associated with secondary PGM inclusions (Fig. 6). Most inclusions are monomineralic, but composite inclusions combining two BMM, BMM–silicate (amphibole, olivine, chlorite, garnet, serpentine) and BMM–PGM (very rare) do occur. Millerite (metal-deficient $Ni_{1-x}S$ with x = 0·02–0·11) containing 2–3 wt % Fe and low Ir and Rh contents (up to 0·53 wt % Ir and 0·20 wt % Rh) is most frequent. Rare pentlandite is Ni rich, and total PGE contents are <0·1 wt %. Very small base metal mineral grains, e.g. native Cu, chalcocite and Sb sulphide (probably stibnite) associated with composite silicate inclusions (amphibole, olivine, pyroxene, chlorite) occur in coarse disseminated chromite from Millionnoe (Fig. 3a).

Table 3: Base metal dominated minerals in chromitite samples of the Kempirsai massif

Mineral	Formula	In chromite	In matrix
Awaruite	Ni_3Fe		x
Chalcocite	Cu_2S	x	
Chromferide	Fe_3Cr_{1-x}	x	x
Covellite	CuS	x	
Copper	Cu	x	x
Cu–Sn alloy	Cu,Sn		x
Dienerite	Ni_3As		x
Heazlewoodite	Ni_3S_2	x	xxx
Maucherite	$Ni_{11}As_8$		x
Millerite	NiS	xxx	xx
Nickeline	NiAs		x
Orcélite	$Ni_{5-x}As_2$		x
Pentlandite	$(Fe,Ni)_9S_8$	x	xx
Pyrite	FeS_2		x
Pyrrhotite	$Fe_{1-x}S$		x
Siegenite	$(Ni,Co)_3S_4$		x
Sphalerite	ZnS		x
Stibnite	Sb_2S_3	x	

Abundances: xxx, frequent; xx, moderately abundant; x, rare.

Base metal minerals in silicate matrix associated with serpentine

Awaruite, Ni_3Fe, is a relatively rare mineral in MOF chromitites and occurs as composite grains up to 40 μm in size with Ni sulphides in the serpentine matrix. Small amounts of native copper and of Cu–Sn alloys (5–20 wt % Sn) are observed in association with chromferide and Ni sulphides. Chromferide, cubic Fe–Cr alloy (Anthony *et al.*, 1990), forms euhedral, anhedral and lamellar grains and is restricted to brecciated chromitites, and to inclusion-rich chromite in chromite–amphibole veins. It contains 87–89 wt % Fe and 9–10 wt % Cr, resulting in a chemical formula of Fe_3Cr_{1-x} ($x=0{\cdot}65$). A formula for Fe_3Cr_{1-x} with $x=0{\cdot}6$ was proposed by Novgorodova *et al.* (1986) for chromferide at the type locality in the southern Urals.

Sulphides and arsenides of Ni are abundant in cracks in chromite, and as grains and aggregates in serpentine (Fig. 6). Heazlewoodite with up to 5 wt % Co and 1 wt % combined Ir and Rh is common. Matrix millerite in MOF chromitite is sometimes slightly enriched in Fe, and depleted in PGE compared with millerite included in chromite. It often replaces heazlewoodite. In BAT chromitite, interstitial millerite carries as much as 0·9 wt % Ir. Pentlandite fills cracks in chromite, and also forms rims around orcélite. Co-bearing varieties (up to 14 wt % Co) occur as cores surrounded by Co-free pentlandite. Ir contents are constantly higher (up to 1 wt %) than in inclusion pentlandite. Pyrrhotite is very rare, and found only as a late, secondary phase in serpentine. Nickel arsenides generally are of secondary origin. They form grains up to 0·25 mm in size which are either homogeneous or composite. Maucherite is more frequent than orcélite. Maucherite, $Ni_{11}As_8$, may carry small inclusions of nickeline, NiAs. Orcélite, $Ni_{5-x}As_2$, rarely occurs as isolated crystals ranging from 5 to 25 μm, but more frequently forms composite grains with Ni sulphide. Small amounts of Ir and Rh are usually detectable in Ni arsenides: maximum values are 1·8 wt % Ir and 0·5 wt % Rh.

FLUID INCLUSIONS IN CHROMITE

Fluid inclusions are generally rare in chromian spinel of ophiolitic chromitites, frequently overlooked, and therefore little work has been done on them (Anthonioz & Correa, 1974; Johan & Le Bel, 1978; Johan *et al.*, 1982, 1983; Dunlop & Fouillac, 1986; McElduff, 1989).

Chromian spinels in New Caledonian, Cyprus and Oman ophiolites are reported to carry primary, pseudosecondary and secondary, two-phase, low-saline aqueous inclusions with variable CH_4 and CO_2. Raman spectroscopy of the gas phase of fluid inclusions in Cyprus chromitites revealed the presence of pure hydrogen (McElduff, 1989). Fluids extracted from Oman chromites have δD values typical of mantle fluids (–53 to –79‰; Dunlop & Fouillac, 1986).

Fluid inclusions are extremely rare and difficult to observe in thin section. In some samples of taxitic and densely disseminated chromitite of both the MOF and BAT, trails of small fluid inclusions, usually monophase, have been observed, whereas nodular types seem to be almost inclusion free. In amphibole–chromite vein-type rock, however, chromite in places contains numerous fluid inclusions which form trails or occur solitary. Three types are distinguished from textural observations (Fig. 3c–f, Fig. 8):

(1) 'Primary' inclusions in the sense of Roedder (1984) are scattered in many chromite crystals both in vein-type and massive chromites. They are hosted by euhedral negative crystal-shaped or rounded cavities and reach 5 μm in size. The most common are one-phase (V?) but two-phase (L + V) inclusions also occur. Occasionally, cracks originate from larger primary inclusions, indicating natural decrepitation.

(2) Large (up to 50 μm) two-phase (L + V), often multifaceted, negative crystal-shaped, euhedral inclusions occur in clusters and trails only in vein-type chromite (Fig. 3e). In such inclusions vapour bubbles occupy ~20–30% of the volume of the inclusions. Clusters of large type (2) inclusions are occasionally surrounded by a network of very small (<5 μm) inclusions which are oriented in two directions outlining the (111) spinel morphology (Fig. 3e). Such inclusions are tabular or elongate and sometimes bent. Trails containing type (2) inclusions are straight or curved, and occasionally form polygonal networks, probably outlining the margins of pre-existing chromite cores before overgrowth. Similar trails also contain numerous solid inclusions (amphibole, chlorite, serpentine, BMM). The majority of large inclusions have features typical of secondary inclusions. In a few cases, however, large fluid inclusion populations occupy the central part of chromite grains and are surrounded by inclusion-free chromite rims. This suggests trapping of fluid during chromite growth, thus implying a 'pseudosecondary' nature of the inclusions (Fig. 3c and d). Microthermometric investigations are very difficult, because of the opaqueness of chromite and the resulting necessity to work with very thin double polished thin sections that tend to break easily. Measurements on larger type (2) inclusions indicate moderately saline aqueous fluids without detectable CO_2. Salinities are comparatively high (10–15 wt % NaCl equivalent), but values as low as 2–3 wt % NaCl equivalent were also measured, corresponding to densities of 0·71–0·87 g/cm^3. Homogenization temperatures are 305 ± 10°C into the liquid phase. Temperatures of eutectic melting could not be observed. The presence of complex salts including Na, Ca and K chlorides and sulphates is indicated by qualitative microprobe measurements of decrepitated inclusions, where salts tend to form thin coatings along inclusion walls.

(3) Elongate (5–10 μm), almost tubular two-phase L + V inclusions form trails and clusters at chromite margins. Some show features indicative of necking. Other inclusions are very irregular in shape and one- or two-phase. This group is interpreted as secondary inclusions trapped during recrystallization of chromite.

Quantification of the fluid species

Preliminary crush–leach experiments carried out on fluid inclusion-rich chromite indicate predominance of Na over K (Na/K, 3·5–8·5). Chlorine, sulphate and fluorine are the major anion species (Cl/SO_4, 0·4–0·8; Cl/F, 0·7–300; Melcher *et al.*, 1997). The fluid in these samples has rather light δD values (–64 and –86‰).

The gas composition in small pieces of handpicked chromite was measured using a quadrupole mass spectrometer attached to a crushing chamber. Gas compositions are highly variable and show high hydrogen contents (Table 4). As expected from microthermometric investigations, samples bearing type (2) inclusions are H_2O dominated (<95 mol %), with minor contents of CO_2 (<1 mol %), N_2 (<0·7 mol %), hydrocarbons and a sulphur species. All these samples show relatively high hydrogen contents (3–58 mol %). Samples of massive chromite lacking amphibole from the Molodezhnoe mine are much lower in total gas contents and are hydrogen dominated.

The high amounts of hydrogen detected in chromite are surprising and might be explained in several ways. Hydrogen may be attached to the chromite lattice; it may be present as gaseous species in fluid inclusions (McElduff, 1989), or it may be adsorbed at the metallic sample holder and released during the cracking process as a result of mechanical strain. The last point cannot be further discussed here. Raman and IR spectroscopic investigations gave no evidence of hydrogen within type (2) inclusions. The other inclusion types are too small to be analysed with Raman spectroscopy. Thus, hydrogen gas most probably is not present in the same inclusions as the aqueous solution, but is either restricted to very small, secondary inclusions or adsorbed onto the spinel phase. Hydrogen was detected by ERDA analysis (elastic recoil detection analysis; Sweeney *et al.*, 1997) in fluid inclusion-rich chromite from the Diamond Pearl mine,

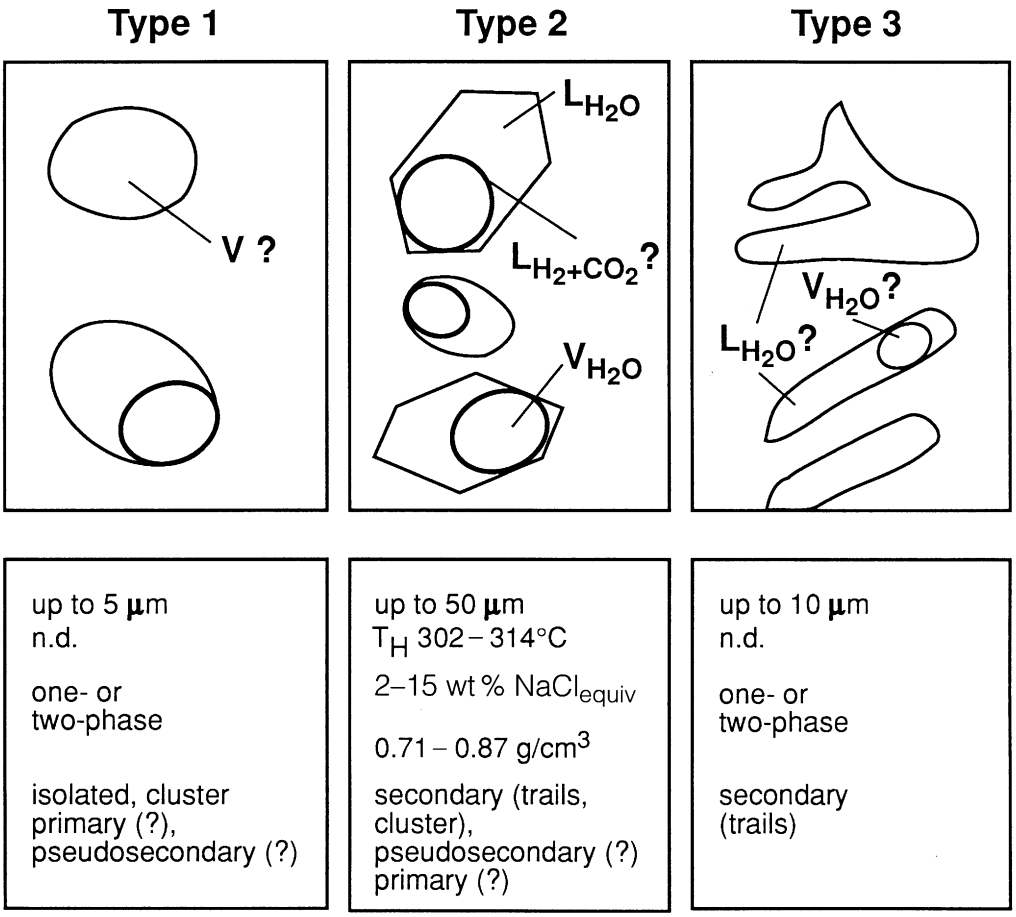

Fig. 8. Textural types of fluid inclusion populations in chromite of the Kempirsai Massif.

Table 4: Composition of fluid phases in purified chromite samples from the Kempirsai Massif

Sample:	93/13B	93/13C	287/6	93/42	93/24
Rock type:	amp–chr	amp–chr	amp–chr	MOF massive	BAT massive
Weight (mg):	148	136	151	158	76
Gas content (cm^3/mg):	0·137	0·137	0·052	0·016	0·137
H_2O (mol %)	40·64	95·44	69·68	26·89	82·88
H_2 (mol %)	58·30	2·92	22·90	69·54	11·59
CH_4 (mol %)	0·10	0·23	5·71	1·14	3·15
C_2H_6 (mol %)	—	0·022	0·033	0·113	0·102
C_3H_8 (mol %)	0·11	0·10	0·15	0·16	0·16
N_2 (mol %)	0·13	0·16	0·74	0·60	0·11
CO (mol %)	0·25	0·30	—	—	0·45
CO_2 (mol %)	0·47	0·69	0·71	1·48	1·44
H_2S (mol %)	—	0·0029	0·0041	0·0049	0·0026
SO_2 (mol %)	—	0·0025	0·0048	0·0071	0·0032

amp–chr, amphibole–chromite rock, Main Ore Field; MOF massive, serpentinized massive chromitite, Main Ore Field; BAT massive, chloritized massive chromitite from Stepninsk, Batamshinsk-type chromitite.

but not in inclusion-free samples. Inclusion-rich chromite contains between 78 and 411 p.p.m. H, whereas inclusion-free chromite contains <30 p.p.m. H. According to the experimental set-up (analysed volume is 10 μm × 10 μm, <0·2 μm depth; R. Sweeney, personal communication 1997), it is highly unlikely that hydrogen was released from fluid inclusions. H_2 gas, being a common fluid species in many hydrothermal fluids, is produced during serpentinization of ultramafic rock (Thayer, 1966). The reaction proposed by Dick (1974),

$$3Fe_2SiO_4 + 2H_2O = 2Fe_3O_4 + 3SiO_2 + 2H_2$$

does not explain the production of a H_2-rich fluid, because the right-hand side of the reaction is the oxidized side. However, hydrogen was found in boreholes drilled through serpentinized ultramafic rocks in the Urals (Betechtin, 1961), and could be detected by Raman analysis in discrete fluid inclusions within pyroxene formed during Alpine metamorphism in the Malenco peridotite, Italy (Peretti *et al.*, 1992). Sulphate-dominated fluids were shown to occur in oxidized serpentinites under upper greenschist–lower amphibolite facies conditions, and are capable of mobilizing significant amounts of sulphides (Frost, 1985).

TEXTURAL SETTING OF INCLUSIONS IN CHROMITE

Inclusions in massive and disseminated chromite of the MOF

High-Cr, low-Al spinels in the MOF cover a small range in *cr*-number and *mg*-number, and have low Ti contents and variable $Fe^{3+}/\Sigma R^{3+}$ values (Fig. 2). Highly magnesian silicates (Am>Ol>Cpx, Opx>Ph; *mg*-number >95) frequently form euhedral or anhedral inclusions in non-fractured and fractured chromite. Some samples are dominated by one silicate alone (Am, Ol, Cpx); others show polyphase silicate inclusions within massive chromite. A common 'stable' association is Cpx + Am. Secondary inclusion silicates comprise serpentine and chlorite as rims around olivine, amphibole and pyroxenes. Complete replacement of the precursor phases also occurs. Frequent associations of primary and secondary minerals include Ol + Srp, Cpx + Srp and Am + Chl. One single occurrence of euhedral uvarovite included in chromite is reported (Fig. 5). Uvarovite is associated with amphibole that is partly replaced by chlorite, and contains a minute inclusion of Ni sulphide. Although anhedral, this particular inclusion cannot have formed in equilibrium with chromite. This underlines the dilemma encountered when studying inclusions in chromite: which inclusions formed earlier than chromite, which formed in equilibrium with chromite, which formed later?

Massive and disseminated chromites carry a variety of PGMs. Polyphase inclusions are common, and in ~50% of the polyphase inclusions, amphibole is present. However, olivine, diopside and Na phlogopite are also observed in association with PGM. These comprise euhedral and anhedral phases of the laurite–erlichmanite series, Os–Ir alloys as well as base metal-rich PGE sulphides. A distinctly different PGM assemblage consisting of PGE sulpharsenides, arsenides and base metal–PGE alloys is associated with serpentine veinlets or with cracks in chromite and has not been found in unaltered chromite. Ni- and Cu-rich sulphides and arsenides lacking significant PGE are rare as inclusions in unaltered chromite, but are frequent in brecciated chromite. In a few samples, very complex assemblages of 'primary' and 'secondary' phases can be found, e.g. Am + Ol + Cpx + Chl + Ni sulphide (Fig. 3a); Am + Chl + Grt + Ni sulphide; Cpx + Srp + Chl + Ni sulphide.

Amphibole–chromite veins in the MOF

In veins and pods of amphibole–chromite rock at the Diamond Pearl mine, anhedral chromite forms aggregates or inclusions in an amphibole matrix. Such chromites are less magnesian, partly also less chromian compared with massive chromitite, and have lower $Fe^{3+}/\Sigma R^{3+}$ (Fig. 2b). Chromite frequently contains trails of solid inclusions (amphibole, Na phlogopite, chlorite, PGM and BMM), and of fluid inclusions (low to moderately saline aqueous inclusions), which occur either in the same trails with solids, or are present in separate trails and clusters. Central cores of some chromite crystals are scattered with large fluid inclusions that show a pseudosecondary texture (Fig. 3c). Such chromites are overgrown by inclusion-free chromite rims. Many of the fluid inclusions are secondary and were entrapped by (re)crystallizing chromite. Fluid-inclusion rich chromite in amphibole matrix in places is rich in Os–Ir alloy, laurite–erlichmanite and (Ni,Cu,Ir) sulphide, and carries minute crystals of chromferide and polyphase amphibole–chlorite–Ni sulphide inclusions.

The fluid inclusion-rich samples studied lack any serpentine minerals. Chlorite is present, but is an alteration product of amphibole. Amphibole–chromite veins postdate the formation of massive chromitite and dunite wallrocks. Sm–Nd mineral isochron ages of harzburgites, websterites, pyroxenites and gabbros from the Kempirsai Massif gave crystallization ages of 390–420 Ma (Edwards & Wasserburg, 1985; Melcher *et al.*, 1997). $^{39}Ar/^{40}Ar$ cooling ages of vein amphibole of 370 Ma point to an 'early' formation of veins and argue against amphibole crystallization during serpentinization (Melcher *et al.*, 1997). Stable isotopes of amphibole indicate derivation from magmatic mantle fluids. If equilibrium between chromite and amphibole has been obtained, and if these

mineral pairs have not been re-equilibrated in terms of $\delta^{18}O$, isotopic fractionation indicates a maximum temperature of 1000°C (Melcher *et al.*, in preparation; method according to Hoffbauer *et al.*, 1994) for this vein assemblage.

Inclusions in massive and orbicular chromite of the BAT and Stepninsk ore fields

Type 2 (low-Cr, high-Al) spinels of the Batamshinsk, Tagashasai and Stepninsk ore fields carry inclusion assemblages completely different from those in the MOF. Primary high-temperature phases are only rarely preserved. Orbicular chromite from Stepninsk was studied in detail, and was found to carry abundant, round chlorite inclusions with Ti- and Cr-rich hydrogarnet, manganoan ilmenite, sphene and Ca–Ti oxide. Ni arsenides and sulphides are frequently associated with chlorite, but also occur in ferritchromit rims of chromian spinel grains. PGM are rare and consist of euhedral laurite and Os–Ir alloy situated in unaltered chromite cores.

DISCUSSION

Although considerable work has been done on inclusions in chromite in recent years, mainly focused on either silicates or PGM, many aspects are still not fully understood, and the 'podiform chromite enigma' remains largely unresolved. The question disputed at present is, does chromitite hosted in mantle tectonites of ophiolite complexes form solely in high-temperature magmatic systems (the orthomagmatic view), or is it possible to precipitate large amounts of chromite in the presence of fluids, e.g. from interactions of fluids with melts as well?

We shall now demonstrate the usefulness of inclusion assemblages to derive constraints on the genesis of podiform chromite deposits. In this paper, three textural settings have been discussed: (1) inclusions in massive and disseminated chromite of the MOF; (2) the amphibole–chromite veins in the MOF; and (3) inclusions in massive and orbicular chromite of the BAT and Stepninsk ore fields.

In general, silicates and PGM included in podiform chromite are very similar in composition, size and shape. But there are also differences, as has been summarized by Augé & Johan (1988) for chromitites from Oman, Greece, Cyprus and New Caledonia. The major differences in inclusion mineralogy between Kempirsai and many other ophiolitic chromitites are: (1) the predominance of amphibole as the silicate phase (similar to Semail, Oman; Augé, 1987); (2) the diversity of 'primary' PGM with abundant base metal–PGE phases (comparable with Finero and Ojen; Ferrario & Garuti, 1990; Torres-Ruiz *et al.*, 1996); (3) the occurrence of Os–Ir alloys with primary textural characteristics; (4) the occurrence of fluid inclusions in specific types of chromite, namely amphibole-hosted chromite. It should be noted that none of these characteristics is unique to Kempirsai alone, and it seems that it is only the size that distinguishes Kempirsai from other ophiolitic–podiform chromite deposits.

Inclusions in chromite from podiform chromitite may be trapped either contemporaneously with chromite precipitation, or considerably later during post-magmatic hydrothermal activity, e.g. during annealing and sintering processes affecting chromite in the presence of a fluid. Excellent reviews on that topic have been given by Lorand & Ceuleneer (1989) and McElduff & Stumpfl (1991). The former presented arguments against post-magmatic entrapment of most silicate inclusions, e.g. compositions of inclusion phases different from hydrothermal alteration products, and textural arrangement of inclusions. Enhanced activity of H_2O was proposed as a result of the abundance of hydroxyl phases. Augé (1987) and Lorand & Ceuleneer (1989) argued in favour of an aqueous fluid phase that evolved independent from the chromite-precipitating magma. Complex inclusion textures as well as peculiar compositions result from reactions occurring inside the inclusions between anhydrous silicates crystallized from the chromite magma and trapped volatile-rich melts or fluids. The presence of phases that are unstable at temperatures close to the chromite liquidus ($\sim 1250 \pm 100$°C) may be explained by reactions inside the inclusions which behaved as closed systems, continuing to temperatures far below the liquidus.

The stability limits of some inclusion phases are known and thus define upper limits of formation for such minerals. According to experimental data, pargasitic amphibole in chromitite may form at temperatures between 950 and 1050°C at oxygen fugacities between the FeO/Fe and the NiO/Ni buffer curves (Wallace & Green, 1991). Above 1050°C, chromian pargasite melts incongruently to form olivine, chromite and melt (Johan & Le Bel, 1978):

$$\text{Cr-pargasite} = \text{chromite} + \text{olivine} + \text{liquid} + \text{vapour}.$$

Amphiboles in mantle rocks are commonly interpreted as having formed during metasomatism, e.g. as a result of the reaction

$$\text{spinel} + \text{diopside} + \text{Al-rich fluid/melt} = \text{amphibole}$$

at pressures <10 kbar (e.g. Francis, 1976; Wallace & Green, 1991). At pressures >15 kbar, silica-undersaturated melts are formed from incongruent melting of amphibole. The maximum depth of sodic amphibole formation in the mantle is constrained to about 100 km (<30 kbar). Experimental evidence shows that the stability of pargasitic amphibole in the mantle depends upon the

mantle H_2O content and bulk-rock composition (Wallace & Green, 1991).

The sodium equivalent of phlogopite has frequently been reported from podiform chromite deposits, such as New Caledonia (Johan, 1986), Troodos (McElduff & Stumpfl, 1991) and Oman (Augé, 1987; Lorand & Ceuleneer, 1989). In podiform chromite of Kempirsai, phlogopite commonly forms solitary, anhedral crystals, indicating entrapment later than much of the euhedral amphibole. It may be produced by reaction of olivine and melt at temperatures below 1010°C (Carman, 1974).

Experimental data on the stability of the 'primary' PGM in chromitites are rare. Augé & Johan (1988) assumed that laurite becomes stable slightly below 1100°C.

Chromian–magnesian chlorite, serpentine and uvarovite are considered relatively low-temperature phases. In agreement with results from serpentinized podiform chromitites world-wide (e.g. Jan & Windley, 1990; Graham *et al.*, 1996) minimum formation temperatures of 500°C are assumed for the assemblage ferritchromit + chlorite + antigorite + chromian garnet.

Mg–Fe exchange geothermobarometry

Fe–Mg partitioning between olivine and spinel is frequently used to derive temperature estimates for peridotites and chromitites (Irvine, 1965, 1967; Jackson, 1969; Fabriès, 1979; Roeder *et al.*, 1979; O'Neill & Wall, 1987; Sack & Ghiorso, 1991). Application of this technique to silicate inclusions in chromitites is problematical because of possible subsolidus re-equilibration processes down to 500°C that severely affect the Fe–Mg distribution in inclusion and host minerals (Lehmann, 1983). This results in unreasonably low temperature estimates for olivine–chromite pairs in most chromitites (e.g. Jan & Windley, 1990). The problem of mineral equilibration can be partly overcome by using mineral compositions from monomineralic rocks, e.g. chromite from chromitite and olivine from dunite (Jackson, 1969). This, however, implies that equilibrium between chromitite and dunite has been attained, which is not consistent with field observations and mineral chemistry.

Representative analyses of spinel, olivine and orthopyroxene from harzburgite, dunite and chromitite of the Main Ore Field are presented in Table 5. Temperature estimates based on the Fe–Mg exchange of spinel and olivine are low (Table 6), especially for highly magnesian (*mg*-number 96–98) olivine inclusions in massive chrome spinel of the orebodies. For chromitite, about 500°C is calculated using the thermodynamic model proposed by Sack & Ghiorso (1991), and about 700°C using the calibration of Ballhaus *et al.* (1991), which is a modified version of the O'Neill & Wall (1987) thermometer. The dunite and harzburgite assemblages of Table 5 give temperatures between 739 and 914°C. Temperatures estimated from Mg–Fe exchange are lower than values calculated from oxygen isotope fractionation between spinel and amphibole in vein-type samples which point to (isotopic) equilibrium at about 1000°C (Melcher *et al.*, 1997, and in preparation).

Given the almost monomineralic nature of the chromitite, with only very minor amounts of magnesian silicates present as inclusions, the composition of chrome spinel is supposed to be very close to its primary, high-temperature value. Thus, in chromitite only olivine changed its Fe–Mg ratio from an unknown value to *mg*-number 96–98. Isopleths constructed for decreasing *mg*-number$_{Ol}$ in T–$f(O_2)$ space show that $Fo_{95–96}$ is in equilibrium with high-Cr spinel at 1000°C, and at 1200°C, Fo_{94} coexists with the given spinel compositions (Fig. 9). Thus, primary olivine compositions were highly magnesian, irrespective of subsolidus re-equilibration processes. Using mineral compositions from nearly monomineralic rocks and following the approach of Jackson (1969) results in high temperature estimates of 1370 and 1395°C (10 kbar) for chromite from chromitite and olivine from dunite (Table 5), respectively.

The composition and stability of chromian spinel are dependent not only on temperature, pressure and bulk composition, but also on oxygen fugacity. An oxygen barometer was proposed by Irvine (1965) and calibrated by Ballhaus *et al.* (1990) using the equilibrium

$$6Fe_2SiO_4 + O_2 = 3Fe_2Si_2O_6 + 2Fe_3O_4.$$

Fe^{2+} and Fe^{3+} values in spinel are calculated from electron microprobe data. Ballhaus *et al.* (1990) found that such recalculated values do not vary significantly from data obtained by Mössbauer spectroscopy. It is assumed that chromite from chromitite did not change its $Fe^{3+}/\Sigma Fe$ and Mg–Fe values upon cooling. Calculated $Fe^{3+}/\Sigma R^{3+}$ values in chromitite from the massive orebodies do not follow oxygen fugacity isobars in diagrams of the type used by Irvine (1965) (Fig. 2b). Moreover, trends for MOF and BAT chromitites are almost perpendicular to such isobars. They trend from low values close to the FMQ buffer curve in harzburgites and dunites, to positive values in massive chromitites. Using the experimental data of Murck & Campbell (1986) and Roeder & Reynolds (1991), $f(O_2)$ in the most oxidized chromites in massive orebodies is within the range of the FMQ and Ni–NiO buffers at 1300°C, and significantly higher if lower temperatures are assumed. The systematic increase in $f(O_2)$ in massive chromitite of the Kempirsai Massif is in contrast to observations from many podiform chromitites. High $f(O_2)$ may partly be attributed to the lack of pyroxene in many of the chromitites and dunites, resulting in a maximum value for $f(O_2)$ in the respective samples (Dick, 1977).

Table 5: Microprobe analyses (wt % and calculated cations) of coexisting olivine (OL), orthopyroxene (OPX) and chromian spinel (SP) from harzburgite (HB), dunite (DU) and chromitite (CH), Main Ore Field, Kempirsai Massif

Mineral:	OL	OPX	SP	OL	SP	OL	OPX	SP	OL	OPX	SP
Sample:	639-1370	639-1370	639-1370	93-37	93-37	AZ1B	AZ1B	AZ1B	185-45	185-37	185-38
Rock:	HB	HB	HB	DU	DU	CH	CH	CH	CH	CH	CH
SiO_2	41·36	55·08	0·01	40·89	0·01	42·47	59·26	0·04	42·19	58·76	0·06
TiO_2	0·02	0·06	0·13	0·00	0·17	0·00	0·00	0·12	0·03	0·03	0·12
Al_2O_3	0·00	2·47	30·11	0·00	7·32	0·00	0·20	8·32	0·06	0·16	8·70
Cr_2O_3	0·00	0·26	34·96	0·04	58·50	0·80	1·12	61·47	1·20	1·32	62·26
FeO_{tot}	10·38	6·77	19·40	7·52	20·51	2·23	1·66	13·48	1·90	1·80	11·99
MnO	0·10	0·12	0·49	0·13	0·52	0·02	0·00	0·33	0·03	0·04	0·48
MgO	48·75	34·18	13·54	50·85	11·33	53·95	37·72	15·80	53·60	37·45	15·90
NiO	0·31	0·07	0·11	0·38	0·23	0·87	0·08	0·12	1·10	0·21	0·20
CaO	0·02	0·20	0·23	0·04	0·00	0·01	0·29	0·00	0·00	0·20	0·00
Na_2O	0·00	0·02	0·00	0·00	0·00	0·00	0·00	0·00	0·00	0·00	0·00
K_2O	0·00	0·03	0·00	0·00	0·00	0·00	0·04	0·00	0·00	0·04	0·00
Total	100·94	99·26	99·00	99·85	98·59	100·35	100·37	99·68	100·11	100·01	99·71
Si	1·006	1·922	0·003	0·995	0·003	1·006	1·995	0·011	1·002	1·990	0·016
Ti	0·000	0·002	0·024	0·000	0·034	0·000	0·000	0·023	0·001	0·001	0·023
Al	0·000	0·102	8·484	0·000	2·309	0·000	0·008	2·511	0·002	0·006	2·620
Cr	0·000	0·007	6·609	0·001	12·377	0·015	0·030	12·444	0·023	0·035	12·577
Fe^{3+}			0·855		1·242			0·977			0·728
Fe^{2+}	0·211	0·198	3·023	0·153	3·348	0·044	0·047	1·909	0·038	0·051	1·835
Mg	1·767	1·778	4·825	1·844	4·519	1·904	1·893	6·030	1·898	1·890	6·055
Mn	0·002	0·004	0·099	0·003	0·118	0·000	0·000	0·072	0·001	0·001	0·104
Ni	0·006	0·002	0·021	0·007	0·050	0·017	0·002	0·025	0·021	0·006	0·042
Ca	0·001	0·007	0·059	0·001	0·000	0·000	0·010	0·000	0·000	0·007	0·000
Na	0·000	0·001	0·000	0·000	0·000	0·000	0·000	0·000	0·000	0·000	0·000
K	0·000	0·001	0·000	0·000	0·000	0·000	0·002	0·000	0·000	0·002	0·000
Total	2·994	4·023	24·002	3·004	24·000	2·987	3·987	24·002	2·985	3·989	24·000
mg-no.	89·33	89·98	61·48	92·34	57·44	97·74	97·58	75·95	98·04	97·37	76·74

Table 6: Temperature and f(O_2) estimates (for P = 10 kbar) based on olivine–chromite–orthopyroxene analyses from Table 5; oxygen fugacities are given for temperature (2)

Sample	Temperature (°C)		Δlog $f(O_2)$ (FMQ)	
	(1)	(2)	(3)	(4)
639-1370 Harzb.	739	815	+0·44	+0·56
93-37 Dunite	889	914	+1·30	+2·57
AZ1B Chromitite	511	746	+3·15	+4·38
185 Chromitite	467	707	+2·93	+4·87

Temperature: (1) Sack & Ghiorso (1991); (2) Ballhaus *et al.* (1991); Δlog $f(O_2)$ (FMQ): (3) Ballhaus *et al.* (1990); (4) Wood (1990).

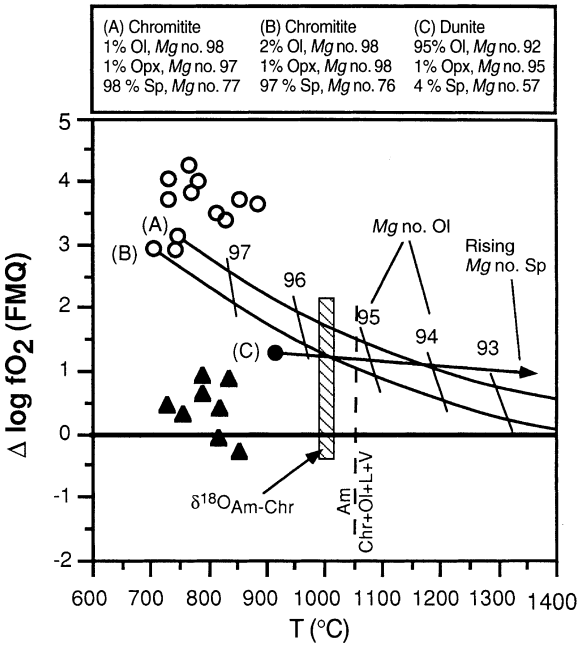

Fig. 9. Variation of temperature and oxygen fugacity for olivine–spinel–orthopyroxene assemblages, calculated using the algorithms after Ballhaus *et al.* (1990, 1991). ○, chromitites; ●, dunites; ▲, harzburgites (note: most chromitites do not contain Opx, and $f(O_2)$ values thus are considered as maximum values). For three assemblages (see Table 5), isopleths are constructed for changing *mg*-number in olivine and chromite, respectively, showing the path along which the rocks equilibrated, assuming that Fe–Mg exchange affected only olivine in chromitite and only chromite in dunite. The amphibole-out curve (Johan & Le Bel, 1978) and a field of temperature estimates based on oxygen isotope fractionation between amphibole and chromite in veins are shown (Melcher *et al.*, in preparation).

The assemblage chromite + forsterite + enstatite is observed in harzburgite host rocks and in massive chromitite from Kempirsai, where these silicates form small inclusions within the spinel phase. If taken at face values, calculated oxygen fugacities for spinel–olivine–orthopyroxene assemblages (Table 5) dramatically increase from harzburgite [$\Delta\log f(O_2)^{FMQ}$ –0·5 to +1 at 700–900°C] to chromitite [$\Delta\log f(O_2)^{FMQ}$ >3 at 700–900°C] (Fig. 9), thus increasing with *cr*-number in spinel. For two chromitites with both olivine and Opx inclusions, isopleths have been constructed and contoured for changes in olivine composition, assuming that volumetrically dominant chromite did not change its composition: if a minimum equilibrium temperature of 1000°C is assumed, oxygen fugacities in chromitite are of the order of one to two log values above the FMQ buffer. Values close to FMQ are reached at temperatures exceeding 1300°C, consistent with the data of Roeder & Reynolds (1991). Wallrock dunite (with rare relict Opx) gives a maximum $f(O_2)$ of +1·5 above FMQ. It is assumed that only volumetrically minor spinel changed to more magnesian compositions during re-equilibration, whereas olivine (*mg*-number 92) remained unchanged; then, $\Delta\log f(O_2)^{FMQ}$ in dunite changes only slightly in a temperature interval between 800 and 1300°C (Fig. 9). It is considered relevant that the back-calculated curves for both chromitite and dunite intersect the amphibole-out curve at 1050°C and $\Delta\log f(O_2)^{FMQ}$ + 1·5.

The oxidation state of metasomatically altered mantle xenoliths bearing amphibole and phlogopite is about one to two log units above FMQ (Wood & Virgo, 1989). This also applies to mantle overlying subduction zones which is infiltrated by water-rich fluids (Brandon & Draper, 1996). Spinel peridotites that have been affected by cryptic metasomatism (no visible mineralogical changes) also record oxygen fugacities about one log unit above FMQ (Hartmann & Wedepohl, 1990). There is appreciable divergence in opinions on the importance of oxygen fugacities in chromite formation. In the Nan Uttaradit ophiolite complex of Thailand, Orberger *et al.* (1995) showed that a special type of chromite crystallized as early segregates from boninitic magmas under strongly reducing conditions in the presence of graphite. Other

chromitites in the same complex, however, formed under elevated water pressures and are characterized by oxygen fugacities close to the FMQ buffer (Orberger *et al.*, 1995). According to Johan *et al.* (1982, 1983) chromite precipitates at 1000°C, 2–5 kbar and low $f(O_2)$ from reaction of a vapour-rich magma with a residual fluid phase. A sudden drop in $f(O_2)$ is explained by appearance of H_2 because of a reaction of a vapour phase with carbon. Although this theory has not been proven in detail experimentally, many arguments presented in this study seem to be in agreement with Johan's model. Low $f(O_2)$ can be inferred for the amphibole–chromite vein rocks at Kempirsai carrying fluid inclusions, and probably hydrogen in the chromite lattice. Elevated $f(O_2)$, however, is assumed for the bulk of the massive chromite ore.

Constraints on magma type and chemistry

Isotope and rare earth element (REE) systematics indicate that the refractory mantle rocks of Palaeozoic ophiolite massifs of the northern and southern Urals formed by progressive extraction of basaltic melt from undepleted mantle (Edwards & Wasserburg, 1985; Sharma *et al.*, 1995; Thalhammer, 1996*b*). Melt separation started in the stability field of garnet lherzolite (depth >80 km), as is indicated by LREE depletion and HREE enrichment of harzburgite, with ~15% of partial melting.

Chromite is a sensitive petrogenetic indicator and can be used to constrain the chemistry of the melt from which the spinel phase precipitated. Based on the Al content of chromite, the Al content of a coexisting melt may be calculated (Maurel & Maurel, 1982) using the formula

$$(Al_2O_3)_{Sp} = 0{\cdot}035(Al_2O_3)^{2{\cdot}42}_{Liquid} \quad (Al_2O_3 \text{ in wt \%}).$$

Calculation of the FeO–MgO ratio of the melt can be done in nearly monomineralic chromitite using the equation of Maurel (1984, cited by Augé, 1987):

$$\ln(FeO/MgO)_{Sp} = 0{\cdot}47 - 1{\cdot}07X\mathrm{Al}_{Sp} + 0{\cdot}64X\mathrm{Fe}^{3+}{}_{Sp} + \ln(FeO/MgO)_{Liquid}$$

with $X\mathrm{Al}_{Sp} = \mathrm{Al}/(\mathrm{Al} + \mathrm{Cr} + \mathrm{Fe}^{3+})$ and $X\mathrm{Fe}^{3+}{}_{Sp} = \mathrm{Fe}^{3+}/(\mathrm{Al} + \mathrm{Cr} + \mathrm{Fe}^{3+})$.

Re-equilibration of Fe and Mg between silicates and chromite may change these values considerably. This may affect the liquid composition calculated for vein-type chromite and BAT chromite, but not for massive, monomineralic MOF chromitite. Such calculations have previously been applied to Oman chromitites (Augé, 1987) and chromitite from Thailand (Orberger *et al.*, 1995). Results for Kempirsai are shown in Table 7. The liquids forming massive chromite of the MOF contained 9–10 wt % Al_2O_3 and had very low FeO–MgO ratios around 0·3–0·5. On the other hand, high-Al spinel in the Batamshinsk ores may have equilibrated with liquids containing 15–16 wt % Al_2O_3 and FeO/MgO values of 0·8–1·0. Parent melts to Oman and Thailand chromitites have higher Al_2O_3 (>11·4 wt %) and MgO/FeO (average 0·62) than MOF chromitite (Augé, 1987; Orberger *et al.*, 1995). Calculated compositions of melts from which MOF chromitites formed are similar to, and even more primitive than, picritic basalt and high-SiO_2, high-MgO boninite. Boninite magmas are Si rich, thus promoting chromite precipitation as a result of polymerization of the melt (Peck & Keays, 1990), and carry elevated Pd and Pt (Hamlyn *et al.*, 1986). BAT chromite may have crystallized from normal basaltic, e.g. MORB-type, liquids.

Table 7: Calculated composition of melts in equilibrium with chromitite from the Kempirsai Massif

	Al_2O_3 liquid[1]	FeO/MgO liquid[2]
MOF massive chromitite	9·0–10·6	0·3–0·5
MOF vein-type chromite	9·6–12·2	0·6–0·8
BAT chromitite	13·5–16·7	0·8–1·0
MOF dunite	8·5–9·1	0·9
Oman chromitite[3]	11·4–16·4	0·62 ± 0·02
Nan Uttaradit chromitite[4]	11·6–12·0	
Boninite[5]	10·6–14·4	0·7–1·4
MORB[5]	~15	1·2–1·6

[1]Maurel & Maurel (1982); [2]Maurel (1984, cited by Augé, 1987); [3]Augé (1987); [4]Orberger *et al.* (1995); [5]Wilson (1989).

Origin of primary PGM and BMM inclusions

Based on their textural position within chromite, solitary and composite, euhedral and anhedral PGM consisting of laurite–erlichmanite, Ir–Rh sulphide, Os–Ir alloy and complex (Ir, Os, Rh, Ni, Cu, Fe) sulphides are considered to be primary inclusions. Textural arguments have been discussed in a number of publications (e.g. Stockman & Hlava, 1984; Prichard *et al.*, 1986, 1994; Augé, 1988; Ferrario & Garuti, 1990; McElduff & Stumpfl, 1990; Thalhammer *et al.*, 1990; Torres-Ruiz *et al.*, 1996). There is a consensus among many researchers that primary PGM formed early as part of the chromite precipitating event. Mechanisms that have been proposed by other researchers, such as subsolidus exsolution from the chromite host and postmagmatic entrapment (sintering) do

not explain the heterogeneous character of inclusion assemblages, such as in Kempirsai. The order of crystallization can be evaluated based on inclusion morphology and chemistry. Euhedral crystal shapes suggest entrapment of solid crystals that formed previous to the chromite. Drop-like textures of inclusions or polygonal boundaries may point to filling of negative crystal cavities in chromite. This implies that such inclusions were in the liquid state when trapped. In Kempirsai chromitites, the presence of PGE-rich liquids may explain many of the complex polyphase inclusions. Distinct boundaries between various PGM in rounded, composite inclusions indicate a stable association. Polyphase PGM may crystallize during subsolidus equilibration, e.g. from PGE-rich liquids, PGE-bearing BM liquids, trapped PGM + PGE-rich liquids, silicates + PGE-rich liquids, or from alkali-, volatile-rich melt + PGE-rich liquid.

In MOF chromites, laurite carries variable Os and Ir contents (Fig. 7b). Euhedral laurites usually carry lower Os than anhedral laurites, which is considered to be primarily an effect of $f(S_2)$. According to the T–$f(S_2)$ diagram compiled from Stockman & Hlava (1984) and Wood (1987) (Fig. 10), laurite crystallizing under high $f(S_2)$ will be enriched in combined Os and Ir compared with laurite formed under relatively lower $f(S_2)$. To equilibrate primary PGE disulphides and to explain the general trend in time of trapping from Ru-rich laurite to Os–(Ir)-rich erlichmanite, an increase in $f(S_2)$ with time should be assumed, if the temperature was constant. Considering a temperature decrease in the system, constant, but also decreasing or increasing sulphur activities can explain the observed mineral assemblages and compositions (arrows in Fig. 10). Compositionally variable Os–Ir alloys are usually associated with a mineral of the laurite–erlichmanite series, with or without PGE–BM sulphide and amphibole. This is unusual for many podiform chromitites, where Os–Ir alloys form in the secondary PGM assemblage as a result of low sulphur activities during serpentinization (Stockman & Hlava, 1984). The buffer curve for various Os contents of the laurite–erlichmanite series is located between Ru–RuS_2 and Os–OsS_2 (Fig. 10). In this region Os–Ir alloy is stable, and it seems that the only factor that controls its composition is the Os:Ir:Ru ratio of the system. Textural features of Ir–Os alloys in chromite suggest that the frequent alloy–sulphide association is not a result of sulphurization of the alloy or desulphurization of the sulphide, but is due to continuous crystallization in equilibrium with laurite–erlichmanite. These phases presumably formed from silicate melt at oxygen fugacities above the FMQ buffer and at temperatures >1000°C; the extension of the buffer curve for the reaction Fa = Po + Mt + Qz (from Barton, 1970) intersects the Ru–RuS_2 buffer at 1000°C and $\log f(S_2) = -4$ (Fig. 10). However, it has been demonstrated in experiments that Os–Ir alloys included in chromite cannot represent early crystallized phases (Peach & Mathez, 1996); they either postdate chromite crystallization, or formed by exsolution. For Ru and Rh, partition coefficients between oxide phase and silicate melt >100 (Capobianco & Drake, 1990; Capobianco *et al.*, 1994) have been experimentally determined, indicating that PGE may partition into spinel and later exsolve. An interesting mechanism explaining the close association of chromite with PGM has been proposed by these workers: in silicate melts, PGE may be present as melt-soluble cluster species (Tredoux *et al.*, 1995). Such clusters may be disproportioned by reaction with chromite as follows:

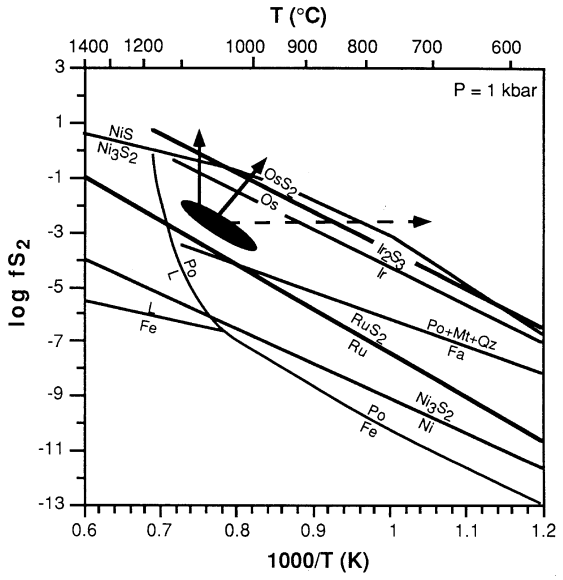

Fig. 10. Diagram of temperature vs activity of sulphur for alloy–sulphide equilibria (after Stockman & Hlava, 1984; Wood, 1987; Ferrario & Garuti, 1990). Field for Os-bearing laurite compositions is explained in the text.

$$Ru_2^{3+} + 0{\cdot}5FeCr_2O_4 \rightarrow Cr^{3+} + Ru^0 + 0{\cdot}5FeRu_2O_4$$

(Capobianco *et al.*, 1994). A PGE cluster (Ru in this case) decomposes in the presence of chromite to form PGE-enriched spinel, alloy and a trivalent cation (Cr, Al, Fe). PGE alloy would crystallize from the neutral species. During subsolidus exsolution reactions, such alloys may act as nucleation sites for PGE exsolving from the spinel lattice, explaining the fact that PGMs included in chromite usually do not show exsolution textures. Capobianco *et al.* (1994) inferred that PGE–sulphide complexes also may react with chromite, producing sulphide inclusions.

Complex and chemically variable Ni- and Ir-rich monosulphides are frequently associated with laurite–erlichmanite and Os–Ir alloys. They have $M_{1-x}S$ stoichiometry close to high-temperature PGE-rich millerite and may be interpreted as products of unmixing of a

BM–PGE-rich sulphide liquid at temperatures lower than those inferred for the crystallization of alloys and laurite–erlichmanite (>1000°C). This implies that sulphur saturation was achieved during chromite formation. However, immiscible Fe + (Ni,Cu) monosulphide melts (Mss) that are segregating from mafic magmas usually crystallize pyrrhotite + pentlandite + chalcopyrite upon cooling. These minerals are not observed as primary inclusions in chromites at Kempirsai. In experiments, Ir-rich Mss converted into Ir-rich thiospinel and pyrrhotite upon cooling below 562°C at sulphur fugacities of the py–po buffer (Evstigneeva & Tarkian, 1996). Ir-rich thiospinel, however, is rarely reported from inclusions in Kempirsai, and the monosulphide seems to be the stable primary phase. According to Fig. 10, Ni, Ir-rich monosulphide is stable at sulphur fugacities similar to, or slightly higher than the Os–OsS_2 buffer, which explains the frequent association with erlichmanite. At temperatures higher than 1050°C, Ni–Ir sulphide may also coexist with Os–Ir alloy.

The formation of similar base metal rich sulphides at Finero, Italy, has been discussed in two ways (Ferrario & Garuti, 1990): formation of an immiscible sulphide liquid, or reactions between H_2S and PGE- and base metal oxide- and (Cl, F, OH, CO)-complexes in volatile-oversaturated silicate melts (Ballhaus & Stumpfl, 1986; Torres-Ruiz *et al.*, 1996). Both models require sulphur saturation. In the fluid model, sulphide liquids are formed by the reactions (Ferrario & Garuti, 1990)

$$H_2S(f) + BMO(L) + O^{2-}(L) = BMS(L) + 2OH^-(Sil)$$

$$H_2S(f) + BMCl(f) + O^{2-}(L) = BMS(L) + 2OH^- + 2Cl^-(Sil)$$

where f is fluid, L is melt, Sil is hydrosilicate, BMO is base metal (PGE) oxide, BMCl is base metal (PGE) chloride and BMS is base metal (PGE) sulphide.

In this case, the composition of the BMS and PGM is controlled not by silicate–sulphide melt distribution coefficients, but by the relative activities of base metals and PGE in the system. The generally low contents of primary sulphides in chromite, their frequent association with alloys, and the lack of Fe-rich Mss indicate that sulphur saturation of the magma was not reached in the early stages of chromite and PGM precipitation. Most PGM appear to have precipitated directly from silicate liquids, and not to have partitioned into Mss. A fully quantitative evaluation of the parameters relevant for evolution in $f(S_2)$–T space and the significance of Mss in podiform chromitite is not possible on the basis of the data available.

The role and source of mantle fluids

Textural and chemical features such as the presence of hydrous silicates in refractory mantle rocks, of olivine replacing orthopyroxene, and of amoeboidal spinel in harzburgite indicate that the mantle in the Kempirsai Massif was pervasively percolated by melts and/or fluids. High amounts of melt are to be expected in areas of high heat flow and steep geothermal gradient, and in the presence of large amounts of fluid depressing the solidus temperatures.

The source of such fluids most probably is a downgoing crustal slab which is subducted underneath oceanic crust of the Kempirsai Massif and an island arc (e.g. the Magnitogorsk arc east of the Kempirsai Massif). Fluids are generated by dehydration of hydrous minerals from subducted material at a depth of 80–125 km (Wilson, 1989). Ascending fluids from the subducted slab trigger first melting in mantle peridotite, because of the inverted geothermal gradient in such settings. Hydrous melts and fluids percolate large volumes of rocks, dissolving chromian diopside and crystallizing orthopyroxene and olivine (Kelemen *et al.*, 1992). Metasomatic replacement of pyroxene-bearing rocks to form dunite has long been acknowledged as the dominant factor in the formation of the platiniferous dunite pipes of the Eastern Bushveld (Schiffries, 1982).

The solubility of silicate components in aqueous fluids equilibrated with mantle mineral assemblages at pressures >10 kbar is substantial. Such fluids are characterized by high alkalinity (Ryabchikov *et al.*, 1982), and thus are capable of transporting high field strength elements (HFSE) and sulphides as hydrosulphide complexes (Ryabchikov, 1991). If the fluids are oxidized and saturated with respect to chlorine or sulphur, they may transport considerable amounts of PGE. The mobility of PGE in the mantle is of importance to understand the enrichment of Ir-group PGE (IPGE) over Pt-group PGE (PPGE), and the abundance of Os–Ir alloys and Ru–Os–Ir sulphides in podiform chromitite. The solubility of IPGE and PPGE in silicate melts increases with increasing oxygen fugacity, especially at values above FMQ (Borisov & Palme, 1995; O'Neill *et al.*, 1995). PPGE are chalcophile in S-saturated MORB liquids, implying that they remain in the mantle source as immiscible sulphide component (Hamlyn *et al.*, 1986). IPGE are siderophile and probably retained in intergranular alloys, as clusters (Tredoux *et al.*, 1995), or present as solid solution in spinel. Remelting of refractory mantle produces S-deficient, PPGE-enriched melts (e.g. boninites), but leaves the IPGE basically unaffected. Mantle restites at Kempirsai are progressively depleted in IPGE from harzburgite to dunite, indicating that IPGE have been mobilized after extraction of silicate melt removing PPGE (Melcher *et al.*, in preparation). The conditions under which IPGE are mobile is a matter of debate; osmium isotope data suggest the mobility of osmium in oxidized, chlorine-rich slab-derived fluids during subduction of oceanic crust (Brandon *et al.*, 1996). IPGE may thus be mobilized from mantle restites by

oxidized fluids; they may be transported as gaseous oxides (Os) or chlorides (Ru) at high temperatures and low sulphur fugacities (Wood, 1987; Mountain & Wood, 1988), and precipitate upon a drop in $f(HCl)$ or $f(O_2)$, or an increase in $f(S_2)$ or $f(H_2O)$. For crystallochemical reasons, the chromite phase acts as a sink for IPGE, which are either dissolved into the spinel lattice and later exsolved (Capobianco & Drake, 1990; Capobianco *et al.*, 1994), or are trapped as solids or liquids during chromite growth. The significance of chlorine for PGE transport and precipitation under hydrothermal conditions has been experimentally demonstrated by Evstigneeva & Tarkian (1996).

Dehydration of subducted sediments and hydrated oceanic crust such as present in the Maksyutov Complex north of Kempirsai (Lennykh *et al.*, 1995; Beane *et al.*, 1996*a*) would allow the release of large amounts of aqueous, alkaline fluid into the mantle wedge, represented by the southeastern part of the Kempirsai Massif. This would induce a second-stage melting process of residual harzburgite forming high-Mg magmas (Duncan & Green, 1987). Picritic and boninitic magmas carry high amounts of Cr if oxygen fugacities are low (Roeder & Reynolds, 1991). High silica and alkali contents cause polymerization of the melt and decrease the number of octahedral sites available for Cr^{3+}, thus precipitating chromite (Dick & Bullen, 1984). A change in $f(O_2)$ as a result of magma mixing or reaction with oxygenated fluid may also drive the liquidus into the field of chromite. Chromite fractionating from such second-stage, fluid-rich magmas in mantle conduits may form dyke-like, discordant orebodies such as those proposed by the mechanisms described by Lago *et al.* (1982) and Leblanc & Ceuleneer (1992). To form very large, almost homogeneous orebodies such as that at Kempirsai, a mechanism is required to constantly precipitate chromite at the same location. Although not manifested by experiments, the idea of Johan *et al.* (1983), namely, interaction of a residual fluid phase with vapour-rich magma, deserves further attention, and gains some support by the observations of immiscibilities, alkali enrichment in inclusions, and fluids trapped during chromite crystallization.

Serpentinization

Serpentinization and associated processes (transformation of PGM, formation of BMM, formation of oxides) at Kempirsai are complex. Similar to many serpentinites associated with ophiolites, serpentinization in Kempirsai was a long-lasting process starting at high temperatures, and low sulphur and oxygen fugacities, which allowed the formation of awaruite and other alloys (Cu–Sn alloy, chromferide), and also of graphite. Continuing serpentinization resulted in the formation of sulphides with decreasing metal:sulphur ratios. A number of reactions occurring in Ni-rich serpentinites have been established by Eckstrand (1975) and Frost (1985). The mineral assemblages observed in Kempirsai chromitites are explained by progressively increasing $f(S_2)$ and $f(O_2)$ with decreasing temperature. Early minerals include pentlandite, pyrrhotite and awaruite, followed by heazlewoodite and millerite. PGM formed during serpentinization occur as trails of composite inclusions in chromite (e.g. serpentine + covellite + BM–PGE sulphide), within serpentine veins in chromite, and rarely in serpentine matrix. BM-bearing alloys, sulphides and arsenides are frequently associated. Along with BMM and secondary PGM, chromian clinochlor, serpentine and occasional uvarovite are included in chromite of some samples. These minerals formed during serpentinization processes and were enclosed by recrystallizing chromite during grain boundary migration. Cr-rich hydrogarnet is present in veinlets and formed during brittle deformation in the temperature range 400–500°C from partial dissolution of chromite. Carbonates are either syngenetic with garnet or postdate garnet formation, indicating high oxygen fugacities and CO_2 pressures in the late stages. Oxygen, carbon and hydrogen isotope analyses of serpentine, chlorite and carbonate minerals in extensively serpentinized samples indicate influence of a meteoric, low-temperature fluid (Melcher *et al.*, in preparation).

A multi-stage model of chromitite formation

Formation of chromite orebodies and included mineral and fluid phases in the Kempirsai Massif is best explained by a multi-stage process:

(1) Basaltic or picritic melts formed in an extensional tectonic setting from partial melting processes affecting relatively fertile peridotite. From such melts, type (2) spinel (high-Al, low-Cr) crystallized in magma chambers in the upper parts of the mantle and at the crust–mantle boundary (Fig. 11), trapping intercumulus silicates and melts. According to Sm–Nd and U–Pb data of mafic cumulates and dyke rocks (Edwards & Wasserburg, 1985; Melcher *et al.*, 1997, and in preparation), mafic melts, and therefore also chromitite associated with them, crystallized in a time span from about 420 to 390 Ma.

(2) After a period of extension, an intra-oceanic subduction zone developed within the Kempirsai Massif (Savelieva & Nesbitt, 1996). Trench sediments, probably representing the southern continuation of the Maksyutov Complex, were subducted underneath oceanic crust of the southeastern Kempirsai Massif at about 380 Ma (Beane *et al.*, 1996*b*) and transformed to eclogite-facies rocks at temperatures of about 600°C and maximum

pressures of 27 kbar (Beane *et al.*, 1996*a*). Fluids released during these reactions metasomatized the already depleted mantle of the MOF within the stability limits of calcic amphibole. Hydrous melting of remaining clino- and orthopyroxene, and more important, metasomatic alteration of restitic orthopyroxene in harzburgite by SiO_2-undersaturated fluid generated a second fluid-rich melt high in Mg, leaving behind even more depleted mantle (concordant dunites), as well as metasomatically enriched mantle (amphibole-bearing harzburgites). Refractory PGE (Os, Ir, Ru) were released from interstitial PGM phases or spinel. As the hydrous melt migrated, chemical disequilibrium between melt and host rock resulted in considerable melt–rock interactions, transforming orthopyroxene in harzburgite to olivine, and thus producing dunite. These dunites were percolated by further fluid-rich melt, becoming richer in silica and fluid with time. In conduits within dunite bodies, chromite started to precipitate over a range of temperature and time, forming massive chromitite and chromite–olivine rock. Components trapped during chromite crystal accumulation and aggregation include magmatic silicates (Ol, Cpx, Opx), hydrous silicates (Amp, Phl), early formed PGM (euhedral laurite), and probably immiscible PGE–BM liquids.

(3) At some later stage, amphibole–chromite veins formed at temperatures around 1000°C and fairly reducing conditions (low $Fe^{3+}/\Sigma R^{3+}$ in spinel). The presence of primary fluid inclusions in chromite is ample evidence for fluid contribution. The fluid was hydrous, moderately saline and carried substantial sulphate, chlorine and CH_4, but only minor CO_2. The inventory of PGM inclusions is similar to that for massive chromitites. In veins, formation of metasomatic amphibole and chromite was contemporaneous, and amphibole cooling ages of 365–370 Ma (Melcher *et al.*, 1997) indicate a close association with the subduction event of Beane *et al.* (1996*b*).

(4) Subsolidus recrystallization and equilibration of chromite must have proceeded to low temperatures, as is evidenced by the entrapment, during serpentinization processes, of low-temperature minerals such as chlorite, serpentine and garnet. Hydrous alteration mainly affected silicate inclusions in BAT chromites, and highly brecciated parts of MOF orebodies (hydrogarnet–carbonate formation). PGE-poor sulphides and arsenides as well as PGE-rich alloys, sulphides, sulpharsenides and arsenides interstitial to chromite or associated with hydrous silicates formed during local mobilization of primary PGM, release of base metals from olivine, and introduction of elements such as arsenic and sulphur. The Kempirsai Massif did not undergo regional metamorphism above greenschist facies to any significant extent. Serpentinization of the uppermost parts of the complex occurred during, or after obduction onto the Russian craton in Late Palaeozoic or Mesozoic times.

CONCLUSIONS

(1) Texturally variable chromian spinel forming large orebodies in the southwestern part of the Kempirsai Massif is chemically homogeneous (*cr*-number 78–85, *mg*-number 63–85). Chromian spinel from small orebodies in the western and northern part of the Massif has lower, and more variable *cr*-number (38–60) and *mg*-number (50–88) values.

(2) Hydrous minerals (amphibole, Na phlogopite) are the most frequent primary silicate inclusions in chromite of the Main Ore Field, and dominate over olivine, diopside and enstatite. All silicates are enriched in Mg (*mg*-number >95) and Cr, as a result of subsolidus reactions with enclosing chromite. Na-rich amphibole is also present as metasomatic reaction products in harzburgite host rocks, and as a matrix mineral to chromite in volumetrically minor vein-type rocks within the orebodies. A different assemblage including chlorite, hydrogarnet, sphene, Mn-ilmenite, zirkelite and apatite prevails in low-grade ores from Stepninsk and Batamshinsk, pointing towards low-temperature recrystallization of chromite (400–500°C).

(3) Mg–Fe values of coexisting chromian spinel and silicates were shifted during subsolidus re-equilibration processes in massive ores. In massive chromitite, oxygen fugacities calculated from chromite–olivine–orthopyroxene equilibria are 1–2 log units above FMQ at 1000°C, and 0·5–1 log unit above FMQ at 1200°C. In dunite hosting chromitite, $f(O_2)$ is about 1·5 log units above FMQ for all temperatures. Formation temperatures close to 1050°C are inferred from the prevalent association with pargasitic hornblende.

(4) Chromite in vein-type amphibole rock carries aqueous, low to moderately saline fluid inclusions with low CO_2 contents. Texturally, primary and pseudosecondary inclusions are distinguished from clearly secondary ones. Hydrogen detected in fluid inclusion-rich chromite most probably is substituted into the chromite lattice.

(5) A suite of platinum-group minerals (mono- and polyphase alloys and sulphides of Ru, Ir, Os) included in chromite of the Main Ore Field records a history of trapping over a wide interval of temperatures and sulphur fugacities. Base metal rich platinum-group element sulphides are associated with primary PGM and hydrous silicate inclusions.

(6) During extensive, surface-controlled serpentinization processes, high- and low-temperature alteration products formed in chromitite. These include

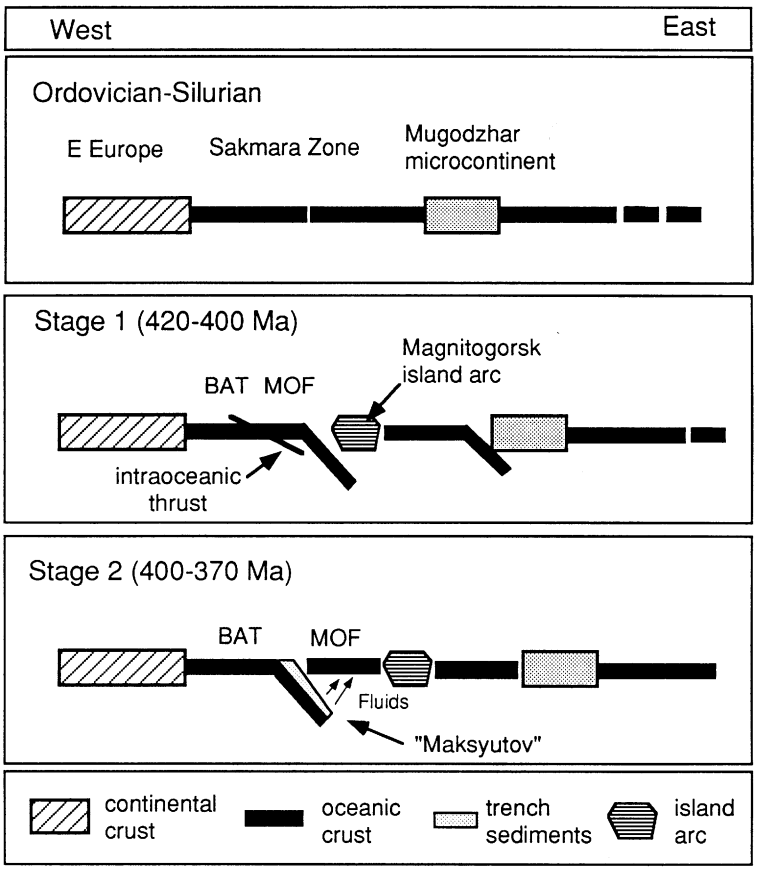

Fig. 11. Schematic cross-section through the western part of the southern Urals in the Palaeozoic. BAT, Batamshinsk (i.e. northwestern part of Kempirsai Massif); MOF, Main Ore Field (i.e. southeastern part of Kempirsai Massif). The figure is based on sketches by Zonenshain *et al.* (1984), Lennykh *et al.* (1995) and Savelieva & Nesbitt (1996).

secondary PGM (sulphides, sulpharsenides, arsenides), base metal alloys, sulphides and arsenides, and silicates (uvarovite, hydro-ugrandite, chlorite, serpentine).

Kempirsai chromitites are in many features very similar to other podiform ophiolitic chromitites; this includes textural as well as geochemical features. Features that distinguish Kempirsai chromitites from classical examples such as those of Oman, New Caledonia, Troodos (Cyprus) and Luobusa (Tibet) are the enormous size of Kempirsai orebodies, and the hydrous regime visible in the inclusion assemblages, which has resulted in a variety of mineral and fluid inclusions. Although many of these minerals presumably formed during subsolidus re-equilibration in solidified chromite, chromite must have trapped components that were not miscible with high-Mg, low-Al melt from which chromite precipitated. These components include BM–PGE-rich liquids or fluids, and hydrous, alkali-rich liquids or fluids. Oxidizing conditions in chromitite and dunite, calculated even for high temperatures (1200°C), are not compatible with pure magmatic processes within anhydrous upper mantle. Keeping this in mind, the genesis of the orebodies may be explained by interaction of a metasomatic alkali-rich mantle fluid or hydrous melt derived from subducted crust, with high-Mg, low-Al melt. This fluid is still preserved in late-stage amphibole–chromite veins. Although there is experimental evidence for the formation of chromite at temperatures of 1250 ± 100°C and $f(O_2)$ around ± 1 log units from the FMQ buffer from 'dry' melts (e.g. Irvine, 1977; Murck & Campbell, 1986; Roeder & Reynolds, 1991), no experimental data are available which could be applied to chromite genesis at Kempirsai. Fluids and fluid-rich melts clearly have played a significant role here and the possibility of lower temperatures of formation for chromite (<1100°C) must be accepted—at least as a feasible alternative.

Small, Al-rich chromite bodies occurring in the upper part of the mantle, and in the transition zone close to the crust–mantle boundary, are explained by fractional crystallization of chromite from basaltic magma derived from partial melting of fertile lherzolite. The giant Al-poor chromite orebodies of the Main Ore Field, hosted by refractory and metasomatized mantle rocks, are restricted to the upper-mantle tectonite sequence of the southwestern part of the massif. Chromites record a complex history in a supra-subduction zone tectonic setting. Fluids released from subducted crust metasomatized the depleted mantle in the mantle wedge above a subducted slab. Hydrous high-Mg, high-Si melts are formed in a process of second-stage melting. Such melts coalesce during their ascent in channels. Along channels, harzburgites are transformed to dunite during extensive melt–rock (Zhou *et al.*, 1994) and fluid–rock interaction; this process causes replacement of orthopyroxene by olivine, and increases the silica content in the liquid. Monomineralic chromitite may then precipitate within the channels. This model explains the macroscopic observation that chromitites frequently postdate dunites that on the other hand grade laterally into harzburgites. The giant size of the Kempirsai orebodies may thus be attributed to several factors: the enormous amounts of volatiles released from a hydrated crust, most probably containing considerable amounts of sediments; intra-oceanic subduction, with fluids affecting already depleted oceanic mantle; and extensional tectonics in the supra-subduction zone (Fig. 11) producing pathways for migrating melts. The genesis of the giant Kempirsai chromite orebodies thus emerges as the result of polyphase processes involving magmatism, fluid regimes and tectonics.

ACKNOWLEDGEMENTS

We thank C. Ballhaus, V. Distler, A. Genkin, J. Konzett, B. Saini-Eidukat, Z. Johan and O. Thalhammer for stimulating discussions and constructive criticism. The paper benefited from careful reviews by B. R. Frost, M.-F. Zhou, Z. Johan and C. Ballhaus. This paper summarizes the results of a co-operative research project conducted jointly by the Institute of Geological Sciences, University of Leoben, and the Institute for the Geology of Ore Deposits, Russian Academy of Sciences, Moscow (IGEM; Professor V. Distler). The project was financed by the Austrian National Science Fund (FWF), Vienna, through Grant 8905 TEC to E. F. Stumpfl. G. Fetisov, President of Donskoi Kombinat, the operating company at Kempirsai, generously provided access to mines and drillcore storage facilities. Chief geologist G. A. Elpashev introduced us to the local geology. The help of Helmut Mühlhans, Chief Technician at the Institute of Geological Sciences, Leoben, with sample preparation and microprobe analysis has been invaluable. We are also grateful to W. Prochaska, Leoben, for carrying out crush–leach experiments on chromite samples; to R. Dobrozemsky, for putting at our disposal mass spectrometric facilities at the Seibersdorf Research Centre; to G. Hoinkes, for the use of the Linkam fluid-inclusion stage at the Institute for Mineralogy, University of Graz; to R. J. Sweeney, for hydrogen analyses on chromite samples using ERDA at the National Accelerator Centre, South Africa.

REFERENCES

Anthonioz, P. M. & Correa, A. V., 1974. Inclusions fluides dans la chromite. Cas des chromites podiformes d'age précambrien au Portugal du Nord-Est. *Comptes Rendues Hebdomadaires des Séances de l'Académie de Science* **278,** 3271–3273.

Anthony, J. W., Bideau, R. A., Bladh, K. W. & Nichols, M. C., 1990. *Handbook of Mineralogy. Volume I: Elements, Sulfides, Sulfosalts*. Tucson, AZ: Mineral Data Publishing.

Augé, T., 1987. Chromite deposits in the northern Oman ophiolite: mineralogical constraints. *Mineralium Deposita* **22,** 1–10.

Augé, T., 1988. Platinum-group minerals in the Tiébaghi and Vourinos ophiolitic complexes: genetic implications. *Canadian Mineralogist* **26,** 177–192.

Augé, T. & Johan, Z., 1988. Comparative study of chromite deposits from Troodos, Vourinos, North Oman and New Caledonia ophiolites. In: Boissonnas, J. & Omenetto, P. (eds) *Mineral Deposits within the European Community*. Berlin: Springer, pp. 267–288.

Ballhaus, C. & Stumpfl, E. F., 1986. Sulfide and platinum mineralization in the Merensky Reef: evidence from hydrous silicates and fluid inclusions. *Contributions to Mineralogy and Petrology* **94,** 193–204.

Ballhaus, C., Cornelius, M. & Stumpfl, E. F., 1988. The Upper Critical Zone of the Bushveld Complex and the origin of the Merensky-type ores—a discussion. *Economic Geology* **83,** 1082–1091.

Ballhaus, C., Berry, R. F. & Green, D. H., 1990. Oxygen fugacity controls in the Earth's upper mantle. *Nature* **348,** 437–440.

Ballhaus, C., Berry, R. F. & Green, D. H., 1991. High-pressure experimental calibration of the olivine–orthopyroxene–spinel geobarometer: implications for the oxidation state of the upper mantle. *Contributions to Mineralogy and Petrology* **107,** 27–40.

Barton, P. B., 1970. Sulfide petrology. *Mineralogical Society of America Special Paper* **3,** 187–198.

Beane, R. J., Liou, J. G., Coleman, R. G. & Leech, M. L., 1996*a*. Petrology and retrograde *P–T* path for eclogites of the Maksyutov Complex, southern Ural Mountains, Russia. *Island Arc* **4,** 254–266.

Beane, R. J., Liou, J. G. & Connelly, J. N., 1996*b*. Evidence for Devonian eclogite-facies metamorphism in the Maksyutov Complex, southern Ural Montains, Russia. *Geological Society of America, Abstracts with Programs* **28,** A-170.

Betechtin, A. G., 1961. Mikroskopische Untersuchungen an Platinerzen aus dem Ural. *Neues Jahrbuch für Mineralogie, Abhandlungen* **97,** 1–39.

Bliss, N. W. & MacLean, W. H., 1975. The paragenesis of zoned chromite from central Manitoba. *Geochimica et Cosmochimica Acta* **39,** 973–990.

Borisov, A. & Palme, H., 1995. The solubility of Ir in silicate melts: new data from experiments with $Ir_{90}Pt_{10}$ alloys. *Geochimica et Cosmochimica Acta* **59,** 481–487.

Boudreau, A. E., Mathez, E. A. & McCallum, I. S., 1986. Halogen geochemistry of the Stillwater and Bushveld Complexes: evidence

for transport of the platinum-group elements by Cl-rich fluids. *Journal of Petrology* **27,** 967–986.

Brandon, A. D. & Draper, D. S., 1996. Constraints on the origin of the oxidation state of mantle overlying subduction zones: an example from Simcoe, Washington, USA. *Geochimica et Cosmochimica Acta* **60,** 1739–1749.

Brandon, A. D., Creaser, R. A., Shirey, S. B. & Carlson, R. W., 1996. Osmium recycling in subduction zones. *Science* **272,** 861–864.

Cabri, L. J., 1981. Platinum-Group Elements: mineralogy, geology, recovery. *Canadian Institute of Mining and Metallurgy Special Volume 23*. Montreal: Canadian Institute of Mining and Metallurgy, 267 pp.

Capobianco, C. J. & Drake, M. J., 1990. Partitioning of ruthenium, rhodium, and palladium between spinel and silicate melt and implications for platinum group element fractionation trends. *Geochimica et Cosmochimica Acta* **54,** 869–874.

Capobianco, C. J., Hervig, R. L. & Drake, M. J., 1994. Experiments on crystal/liquid partitioning of Ru, Rh and Pd for magnetite and hematite solid solutions crystallized from silicate melt. *Chemical Geology* **113,** 23–43.

Carman, J. H., 1974. Synthetic sodium phlogopites and its two hydrates. *American Mineralogist* **59,** 261–273.

Cassard, D., Nicolas, A., Rabinovitch, M., Moutte, J., Leblanc, M. & Prinzhofer, A., 1981. Structural classification of chromite pods in southern New Caledonia. *Economic Geology* **76,** 805–831.

Deer, W. A., Howie, R. A. & Zussman, J., 1982. *Rock-forming Minerals. Volume 1A, Orthosilicates*, 2nd edn. Harlow, UK: Longman.

Dick, H. J. B., 1974. Terrestrial nickel–iron from the Josephine peridotite, its geologic occurrence, associations and origin. *Earth and Planetary Science Letters* **24,** 291–298.

Dick, H. J. B., 1977. Partial melting in the Josephine peridotite: 1, The effect on mineral composition and its consequences for geobarometry and geothermometry. *American Journal of Science* **277,** 801–832.

Dick, H. J. B. & Bullen, T., 1984. Chromian spinel as a petrogenetic indicator in abyssal and alpine-type peridotites and spatially associated lavas. *Contributions to Mineralogy and Petrology* **86,** 54–76.

Distler, V. V., Volchenko, J. A., Kryachko, V. V., Elpashev, G. A. & Merkulov, G. A., 1989. Platinum-group minerals in chromitites of the Kempirsai massif, South Ural. *Report of the Russian Academy of Science* **11,** 113–117 (in Russian).

Dmitrenko, G. G., 1994. *Platinum-group Minerals of Alpine-type Ultramafics*. Magadan, 134 pp. (in Russian).

Dobretsov, N. L., Shatsky, V. S., Coleman, R. G., Lennykh, V. I., Valizer, P. M., Liou, J., Zhang, R. & Beane, R. J., 1996. Tectonic setting and petrology of ultrahigh-pressure metamorphic rocks in the Maksyutov Complex, Ural Mountains, Russia. *International Geology Reviews* **38,** 136–160.

Dobrozemsky, R., 1972. Experience with a computer program for residual gas analyses. *Journal of Vacuum Sciences and Technology* **9**(1), 220–233.

Dobrozemsky, R., 1990. Calibration of vacuum systems by gas quantities. *Vacuum* **41,** 2109–2111.

Duncan, R. A. & Green, D. H., 1987. The genesis of refractory melts in the formation of oceanic crust. *Contributions to Mineralogy and Petrology* **96,** 326–342.

Dunlop, H. M. & Fouillac, A. M., 1986. Isotope geochemistry of Oman basic–ultrabasic rocks and chromite deposits. In: Gallagher, M. J., Ixer, R. A., Neary, C. R. & Prichard, H. M. (eds) *Metallogeny of Basic and Ultrabasic Rocks*. London: Institution of Mining and Metallurgy, pp. 291–304.

Eckstrand, O. R., 1975. The Dumont Serpentinite: a model for control of nickeliferous opaque mineral assemblages by alteration reactions in ultramafic rocks. *Economic Geology* **70,** 183–201.

Edwards, R. L. & Wasserburg, G. J., 1985. The age and emplacement of obducted oceanic crust in the Urals from Sm–Nd and Rb–Sr systematics. *Earth and Planetary Science Letters* **72,** 389–404.

Evans, B. W. & Frost, B. R., 1975. Chrome-spinel in progressive metamorphism—a preliminary analysis. *Geochimica et Cosmochimica Acta* **39,** 959–972.

Evstigneeva, T. & Tarkian, M., 1996. Synthesis of platinum-group minerals under hydrothermal conditions. *European Journal of Mineralogy* **8,** 549–564.

Fabriès, J., 1979. Spinel–olivine geothermometry in peridotites from ultramafic complexes. *Contributions to Mineralogy and Petrology* **69,** 329–336.

Ferrario, A. & Garuti, G., 1990. Platinum-group mineral inclusions in chromitites of the Finero mafic–ultramafic complex (Ivrea-Zone, Italy). *Mineralogy and Petrology* **41,** 125–143.

Francis, D., 1976. The origin of amphibole in lherzolite xenoliths from Nunivak Island, Alaska. *Journal of Petrology* **17,** 357–378.

Frost, B. R., 1985. On the stability of sulfides, oxides, and native metals in serpentinite. *Journal of Petrology* **26,** 31–63.

Ganguly, J., 1976. The energetics of natural garnet solid solutions: II. Mixing of the calcium silicate end-members. *Contributions to Mineralogy and Petrology* **55,** 81–90.

Garuti, G., Gazzotti, M. & Torres-Ruiz, J., 1995. Iridium, rhodium, and platinum sulfides in chromitites from the ultramafic massifs of Finero, Italy, and Ojén, Spain. *Canadian Mineralogist* **33,** 509–520.

Graham, I. T., Franklin, B. J. & Marshall, B., 1996. Chemistry and mineralogy of podiform chromitite deposits, southern NSW, Australia: a guide to their origin and evolution. *Mineralogy and Petrology* **57,** 129–150.

Haggerty, S. E., 1991. Oxide mineralogy of the upper mantle. In: Lindsley, D. H. (ed.) *Oxide Minerals: Petrologic and Magnetic Significance. Mineralogical Society of America, Reviews in Mineralogy* **25,** 355–416.

Hamlyn, P. R., Keays, R. R., Cameron, W. E., Crawford, A. J. & Waldron, H. M., 1986. Precious metals in magnesian low-Ti lavas: implications for metallogenesis and sulfur saturation in primary magmas. *Geochimica et Cosmochimica Acta* **49,** 1797–1811.

Harris, D. C. & Cabri, L. J., 1991. Nomenclature of platinum-group alloys: review and revision. *Canadian Mineralogist* **29,** 231–237.

Hartmann, G. & Wedepohl, K. H., 1990. Metasomatically altered peridotite xenoliths from the Hessian Depression (Northwest Germany). *Geochimica et Cosmochimica Acta* **54,** 71–86.

Heraskov, N. P. & Razumova, V. N., 1967. Ultramafic formations of the Kempirsai massif, South Ural, and associated gabbro–amphibolites. In *Tectonics and Formations*. Moscow: Nauka, pp. 103–141 (in Russian).

Hoffbauer, R., Hoernes, S. & Fiorentini, E., 1994. Oxygen isotope thermometry based on a refined increment method and its application to granulite-grade rocks from Sri Lanka. *Precambrian Research* **66,** 199–220.

Irvine, T. N., 1965. Chromian spinel as a petrogenetic indicator. Part 1. Theory. *Canadian Journal of Earth Sciences* **2,** 648–672.

Irvine, T. N., 1967. Chromian spinel as a petrogenetic indicator. Part 2. Petrologic applications. *Canadian Journal of Earth Sciences* **4,** 71–104.

Irvine, T. N., 1977. Chromite crystallization in the join Mg_2SiO_4–$CaMgSi_2O_6$–$CaAl_2Si_2O_8$–$MgCr_2O_4$–SiO_2. *Carnegie Institution of Washington, Yearbook* **76,** 465–472.

Jackson, E. D., 1969. Chemical variation in coexisting chromite and olivine in chromitite zones of the Stillwater Complex. *Economic Geology Monograph Series* **4,** 41–71.

Jan, M. Q. & Windley, B. F., 1990. Chromian spinel–silicate chemistry in ultramafic rocks of the Jijal Complex, northwest Pakistan. *Journal of Petrology* **31,** 667–715.

Johan, Z., 1986. Chromite deposits in the Massif du Sud ophiolite, New Caledonia: genetic consideration. In: *Chromites. UNESCO's IGCP-197 Project.* Athens: Theophrastos, pp. 311–339.

Johan, Z., 1995. Metallogeny of basic and ultrabasic complexes. Invited lecture, Third Biennial SGA Meeting, Prague.

Johan, Z. & Le Bel, L., 1978. Sur la genèse des couches et podes de chromite dans les complexes ophiolitiques. *Résumé des principaux résultats science et technique, Serv. Geol. Natl* **1978,** 96–99.

Johan, Z., Robert, J. L. & Volfinger, M., 1982. Role of reducing fluids in the origin of chromite deposits from ophiolitic complexes. *Abstracts, Geological Association of Canada* **7,** 58.

Johan, Z., Dunlop, H., Le Bel, L., Robert, J. L. & Volfinger, M., 1983. Origin of chromite deposits in ophiolitic complexes: evidence for a volatile- and sodium-rich reducing fluid phase. *Fortschritte der Mineralogie* **61,** 105–107.

Kamaletdinov, M. A., 1974. *Allochthonous Structures of the Urals*. Moscow: Nauka, 229 pp. (in Russian).

Kelemen, P. B., Dick, H. J. B. & Quick, J. E., 1992. Formation of harzburgite by pervasive melt/rock reaction in the upper mantle. *Nature* **358,** 635–641.

Kravchenko, G. G. & Grigoryeva, I. I., 1986. The Kempirsaisky chromite-bearing massif in the Ural mountains. In: *Chromites. UNESCO's IGCP-197 Project.* Athens: Theophrastos, pp. 23–44.

Kullerud, G. & Yund, R. A., 1962. The Ni–S system and related minerals. *Journal of Petrology* **3,** 126–175.

Lago, B. L., Rabinowicz, M. & Nicolas, A., 1982. Podiform chromite ore bodies: a genetic model. *Journal of Petrology* **23,** 103–125.

Laz'ko, E. E., 1989. Mineral composition in the sequence of the Kempirsai ultramafic massif (North-West Kazakhstan). *Petrology* **3,** 45–49 (in Russian).

Leblanc, M. & Ceuleneer, G., 1992. Chromite crystallization in a multicellular magma flow: evidence from a chromitite dike in the Oman ophiolite. *Lithos* **27,** 231–257.

Legendre, O. & Augé, T., 1986. Mineralogy of platinum-group mineral inclusions in chromitites from different ophiolitic complexes. In: Gallagher, M. J., Ixer, R. A., Neary, C. R. & Prichard, H. M. (eds) *Metallogeny of Basic and Ultrabasic Rocks*. London: Institution of Mining and Metallurgy, pp. 361–372.

Lehmann, J., 1983. Diffusion between olivine and spinel: application to geothermometry. *Earth and Planetary Science Letters* **64,** 123–138.

Lennykh, V. I., Valizer, P. M., Beane, R., Leech, M. & Ernst, W. G., 1995. Petrotectonic evolution of the Maksyutov Complex, southern Urals, Russia: implications for ultrahigh-pressure metamorphism. *International Geology Reviews* **37,** 584–600.

Li, J.-P., O'Neill, H. St. C. & Seifert, F., 1995. Subsolidus phase relations in the system MgO–SiO_2–Cr–O in equilibrium with metallic Cr, and their significance for the petrochemistry of chromium. *Journal of Petrology* **36,** 107–132.

Lorand, J. P. & Ceuleneer, G., 1989. Silicate and base-metal sulfide inclusions in chromites from the Maqsad area (Oman ophiolite, Gulf of Oman): a model for entrapment. *Lithos* **22,** 173–190.

Lorand, J. P. & Cottin, J. Y., 1987. Na–Ti–Zr–H_2O-rich mineral inclusions indicating post-cumulus chrome-spinel dissolution and recrystallization in the Western Laouni mafic intrusion, Algeria. *Contributions to Mineralogy and Petrology* **86,** 251–263.

Malpas, J. & Strong, D. F. A., 1975. A comparison of chrome-spinels in ophiolites and mantle diapirs of Newfoundland. *Geochimica et Cosmochimica Acta* **39,** 1045–1060.

Mathez, E. A., 1989. Interactions involving fluids in the Stillwater and Bushveld Complexes: observations from the rocks. *Reviews in Economic Geology* **4,** 167–179.

Maurel, C. & Maurel, P., 1982. Étude expérimentale de la solubilité du chrome dans les bains silicatés basiques et sa distribution entre liquide et minéraux coexistants: conditions d'existence du spinelle chromifère. *Bulletin Minéralogie* **105,** 640–647.

McElduff, B., 1989. Inclusions in chromite from Troodos (Cyprus) and their petrological significance. Ph.D. Thesis, Montan-Universität Leoben, Austria, 143 pp.

McElduff, B. & Stumpfl, E. F., 1990. Platinum-group minerals from the Troodos Ophiolite, Cyprus. *Mineralogy and Petrology* **42,** 211–232.

McElduff, B. & Stumpfl, E. F., 1991. The chromite deposits of the Troodos Complex, Cyprus—evidence for the role of a fluid phase accompanying chromite formation. *Mineralium Deposita* **26,** 307–318.

Melcher, F., Stumpfl, E. F. & Distler, V., 1994. Chromite deposits of the Kempirsai massif, southern Urals, Kazakhstan. *Transactions of the Institution of Mining and Metallurgy (Section B: Applied Earth Sciences)* **103,** B107–B120.

Melcher, F., Stumpfl, E. F. & Simon, G., 1995. Platinum-group minerals and associated inclusions in chrome spinel of the Kempirsai ultramafic massif, Southern Urals, Kazakhstan. In: Pasava, J., Kríbek, B. & Zák, K. (eds) *Mineral Deposits: From their Origin to their Environmental Impacts. Proceedings of the Third Biennial SGA Meeting, Prague.* Rotterdam: Balkema, pp. 153–156.

Melcher, F., Grum, W. & Stumpfl, E. F., 1996. Ophiolitic–podiform chromite giants in the southern Urals: implications from geochemistry and the role of fluids. *Geological Society of America, Abstracts with Programs* **28,** A92–A93.

Melcher, F., Grum, W., Thalhammer, O. A. R. & Stumpfl, E. F., 1997. Giant chromite deposits and their host rocks, Kempirsai, Urals: an integrated study of precious metals, rare earth elements, stable and radiogenic isotopes, and the composition of fluid inclusions in chromite. In: Papunen, H. (ed.) *Mineral Deposits: Research and Exploration—Where do they Meet? Proceedings of the Fourth Biennial SGA Meeting, Turku.* Rotterdam: Balkema, pp. 479–482.

Miura, Y., Rucklidge, J. & Nord, G. L., Jr, 1981. The occurrence of chlorine in serpentine minerals. *Contributions to Mineralogy and Petrology* **76,** 17–23.

Mogessie, A. & Saini-Eidukat, B., 1992. A review of the occurrence of platinum group elements in the Duluth Complex, Minnesota, U.S.A. *Trends in Mineralogy* **1,** 65–84.

Mountain, B. W. & Wood, S. A., 1988. Solubility and transport of platinum-group elements in hydrothermal solutions: thermodynamic and physical chemical constraints. In: Prichard, H. M., Potts, P. J., Bowles, J. F. W. & Gibb, S. J. (eds) *Geoplatinum '87*. Amsterdam: Elsevier, pp. 57–82.

Murck, B. W. & Campbell, I. H., 1986. The effects of temperature, oxygen fugacity and melt composition on the behaviour of chromium in basic and ultrabasic melts. *Geochimica et Cosmochimica Acta* **50,** 1877–1887.

Nicolas, A. & Prinzhofer, A., 1983. Cumulative or residual origin for the transition zone in ophiolites: structural evidence. *Journal of Petrology* **24,** 188–206.

Nilsson, L. P., 1990. Platinum-group mineral inclusions in chromitite from the Osthammeren ultramafic tectonite body, south central Norway. *Mineralogy and Petrology* **42,** 249–263.

Novgorodova, M. I., Gorshkov, A. I., Trubkin, N. V., Tsepin, A. I. & Dmitrieva, M. T., 1986. New natural intermetallic compounds of iron and chromium—chromferide and ferchromide. *Reports of the Mineralogical Society* **115,** 355–360 (in Russian).

O'Neill, H. St. C. & Wall, V. J., 1987. The olivine–orthopyroxene–spinel oxygen geobarometer, the nickel precipitation curve, and the oxygen fugacity of the earth's upper mantle. *Journal of Petrology* **28,** 1169–1191.

O'Neill, H. St. C., Dingwell, D. B., Borisov, A., Spettel, B. & Palme, H., 1995. Experimental petrochemistry of some highly siderophile elements at high temperatures, and some implications for core

formation and the mantle's early history. *Chemical Geology* **120,** 255–273.

Orberger, B., Friedrich, G. & Woermann, E., 1988. Platinum-group element mineralization in the ultramafic sequence of the Acoje ophiolite block, Zambales, Philippines. In: Prichard, H. M., Potts, P. J., Bowles, J. F. W. & Gibb, S. J. (eds) *Geoplatinum '87*. Amsterdam: Elsevier, pp. 361–380.

Orberger, P., Lorand, J. P., Girardeau, J., Mercier, J. C. C. & Pitragool, S., 1995. Petrogenesis of ultramafic rocks and associated chromitites in the Nan Uttaradit ophiolite, Northern Thailand. *Lithos* **35,** 153–182.

Paktunç, A. D., 1990. Origin of podiform chromite deposits by multi-stage melting, melt segregation and magma mixing in the upper mantle. *Ore Geology Reviews* **5,** 211–222.

Pavlov, N. V. & Grigoryeva, I. I., 1977. Deposits of chromium. In: Smirnov, V. I. (ed.) *Ore Deposits of the USSR, Vol. I*. London: Pitman, pp. 179–236.

Pavlov, N. V., Kravchenko, G. G. & Chuprynina, I. I., 1968. *The Chromites of the Kempirsai Pluton*. Moscow: Nauka, 178 pp. (in Russian).

Peach, C. L. & Mathez, E. A., 1996. Constraints in the formation of platinum-group element deposits in igneous rocks. *Economic Geology* **91,** 439–450.

Peck, D. C. & Keays, R. R., 1990. Geology, geochemistry, and origin of platinum-group element–chromitite occurrences in the Heazlewood River Complex, Tasmania. *Economic Geology* **85,** 765–793.

Perfiliev, A., 1979. Ophiolitic belt of the Urals. *Geological Society of America Map and Chart Series* **MC-33,** pp. 9–12.

Peretti, A., Dubessy, J., Mullis, J., Frost, B. R. & Trommsdorff, V., 1992. Highly reducing conditions during Alpine metamorphism of the Malenco peridotite (Sondrio, northern Italy) indicated by mineral paragenesis and H_2 in fluid inclusions. *Contributions to Mineralogy and Petrology* **112,** 329–340.

Prichard, H. M., Neary, C. R. & Potts, P. J., 1986. Platinum group minerals in the Shetland ophiolite. In: Gallagher, M. J., Ixer, R. A., Neary, C. R. & Prichard, H. M. (eds) *Metallogeny of Basic and Ultrabasic Rocks*. London: Institution of Mining and Metallurgy, pp. 395–414.

Prichard, H. M., Ixer, R. A., Lord, R. A., Maynard, J. & Williams, N., 1994. Assemblages of platinum-group minerals and sulfides in silicate lithologies and chromite-rich rocks within the Shetland ophiolite. *Canadian Mineralogist* **32,** 271–294.

Roberts, S., 1988. Ophiolitic chromitite formation: a marginal basin phenomenon? *Economic Geology* **83,** 1034–1036.

Roedder, E., 1984. Fluid inclusions. *Mineralogical Society of America, Reviews in Mineralogy* **12,** 644 pp.

Roeder, P. L. & Reynolds, I., 1991. Crystallization of chromite and chromium solubility in basaltic melts. *Journal of Petrology* **32,** 909–934.

Roeder, P. L., Campbell, I. H. & Jamieson, H. E., 1979. A re-evaluation of the olivine–spinel geothermometer. *Contributions to Mineralogy and Petrology* **68,** 325–334.

Rucklidge, J. C. & Patterson, G. C., 1977. The role of chlorine in serpentinization. *Contributions to Mineralogy and Petrology* **65,** 39–44.

Ryabchikov, I. D., 1991. Mobilization of metals by aqueous fluids and carbonatitic melts in mantle peridotites. In: Pagel, M. & Leroy, J. L. (eds) *Source, Transport and Deposition of Metals*. Rotterdam: Balkema, pp. 119–121.

Ryabchikov, I. D., Schreyer, W., & Abraham, K., 1982. Compositions of aqueous fluids in equilibrium with pyroxenes and olivines at mantle pressures and temperatures. *Contributions to Mineralogy and Petrology* **79,** 80–84.

Sack, R. O. & Ghiorso, M. S., 1991. Chromian spinels as petrogenetic indicators: thermodynamics and petrological application. *American Mineralogist* **76,** 827–847.

Saini-Eidukat, B., Kucha, H. & Keppler, H., 1994. Hibbingite, γ-$Fe_2(OH)_3Cl$, a new mineral from the Duluth Complex, Minnesota, with implications for the oxidation of Fe-bearing compounds and the transport of metals. *American Mineralogist* **79,** 555–561.

Saveliev, A. A. & Savelieva, G. N., 1991. Ophiolites of the Kempirsai massif: general features of the structural–compositional evolution. *Geotectonics* **6,** 57–75 (in Russian).

Savelieva, G. N. & Nesbitt, R. W., 1996. A synthesis of the stratigraphic and tectonic setting of the Uralian ophiolites. *Journal of the Geologial Society, London* **153,** 525–538.

Schiffries, C. M., 1982. The petrogenesis of a platiniferous dunite pipe in the Bushveld Complex: infiltration metasomatism by a chloride solution. *Economic Geology* **77,** 1439–1453.

Segalovich, V. I., 1973. Geophysical model of the Kempirsai ultramafic massif in light of a new conception of Ural tectonics. *Doklady Russian Academy of Sciences* **213,** 669–672 (in Russian).

Sharma, M., Wasserburg, G. J., Papanastassiou, D. A., Quick, J. E., Sharkov, E. V. & Laz'ko, E. E., 1995. High $^{143}Nd/^{144}Nd$ in extremely depleted mantle rocks. *Earth and Planetary Science Letters* **135,** 101–114.

Shepherd, T. J., 1981. Temperature-programmable, heating–freezing stage for microthermometric analysis of fluid inclusions. *Economic Geology* **76,** 1244–1247.

Smirnova, T. A., 1973. Geochemistry of ultramafics and chrome-spinelides of the Kempirsai massif. Abstract of Ph.D Thesis, Institute of Mineral Resources, Russian Academy of Science, Moscow, 31 pp. (in Russian).

Sokolov, G. A., 1948. Chromites of the Ural, its composition, conditions of formation and distribution. *Reports of the Geological Institute, Russian Academy of Science* **97,** 127 pp. (in Russian).

Spangenberg, K., 1943. Die Chromerzlagerstätte von Tampadel am Zobten. *Zeitschrift für praktische Geologie* **51,** 13–36.

Stockman, H. W. & Hlava, P. F., 1984. Platinum-group minerals in Alpine chromitites from southwestern Oregon. *Economic Geology* **79,** 491–508.

Stowe, C. W., 1987. *Evolution of Chromium Ore Fields*. New York: Van Nostrand–Reinhold, 340 pp.

Stumpfl, E. F., 1986. Distribution, transport and concentration of platinum group elements. In: Gallagher, M. J., Ixer, R. A., Neary, C. R. & Prichard, H. M. (eds) *Metallogeny of Basic and Ultrabasic Rocks*. London: Institution of Mining and Metallurgy, pp. 379–394.

Stumpfl, E. F., 1993. Fluids: a prerequisite for platinum metals mineralization. In: Hach-Ali, F., Torres-Ruiz, J. & Gervilla, F. (eds) *Current Research in Geology Applied to Ore Deposits*. Rotterdam: Balkema, pp. 15–21.

Sweeney, R. J., Prozesky, V. M. & Springhorn, K. A., 1997. Use of the elastic recoil detection analysis (ERDA) microbeam technique for the quantitative determination of hydrogen in materials and hydrogen partitioning between olivine and melt at high pressures. *Geochimica et Cosmochimica Acta* **61,** 101–113.

Talkington, R. W., Watkinson, D. H., Whittaker, P. J. & Jones, P. C., 1984. Platinum-group minerals and other solid inclusions in chromite of ophiolitic complexes: occurrence and petrological significance. *Tschermaks Mineralogische und Petrographische Mitteilungen* **32,** 285–301.

Tarkian, M., Naidenova, E. & Zhelyaskova-Panayotova, M., 1991. Platinum-group minerals in chromitites from the Eastern Rhodope Ultramafic Complex, Bulgaria. *Mineralogy and Petrology* **44,** 73–87.

Thalhammer, O. A. R., Prochaska, W. & Mühlhans, H. W., 1990. Solid inclusions in chrome-spinels and platinum group element concentrations from the Hochgrössen and Kraubath Ultramafic Massifs (Austria). *Contributions to Mineralogy and Petrology* **105,** 66–80.

Thalhammer, T. V., 1996*a*. Association of platinum-group minerals in massive chromite ores of the Kempirsai ophiolitic complex (South

Ural): evidence for mantle metasomatism. *Reports of the Mineralogical Society* **1,** 25–36 (in Russian).

Thalhammer, T. V., 1996*b*. The Kempirsai ophiolite complex, south Ural: Petrology, geochemistry, platinum-group minerals, chromitite deposits. Ph.D. Thesis, Mining University Leoben, 197 pp.

Thayer, T. P., 1966. Serpentinization considered as a constant volume metasomatic process. *American Mineralogist* **51,** 685–710.

Thayer, T. P., 1969. Gravity differentiation and magmatic re-emplacement of podiform chromite deposits. *Economic Geology Monographs* **4,** 132–146.

Torres-Ruiz, J., Garuti, G., Gazzotti, M., Gervilla, F. & Hach-Ali, P. F., 1996. Platinum-group minerals in chromitites from the Ojen lherzolite massif (Serranía de Ronda, Betic Cordillera, Spain). *Mineralogy and Petrology* **56,** 25–50.

Tredoux, M., Lindsay, N. M., Davies, G. & McDonald, I., 1995. The fractionation of platinum-group elements in magmatic systems, with the suggestion of a novel causal mechanism. *South African Journal of Geology* **98,** 157–167.

Volborth, A., Stumpfl, E. F., Tarkian, M. & Housley, R. M., 1985. Examples of Pd–Pt mineralization along the 35 km strike of the Stillwater Reef, Montana, USA. *Canadian Mineralogist* **23,** 319.

Volchenko, J. A. & Vigorov, B. L., 1987. First discovery of platinum-group minerals in the Kempirsai chromitites. Ekaterinburg. *Reports of the Institute of Geology and Geochemistry* **1,** 70–71 (in Russian).

Wallace, M. E. & Green, D. H., 1991. The effect of bulk composition on the stability of amphibole in the upper mantle: implications for solidus positions and mantle metasomatism. *Mineralogy and Petrology* **44,** 1–19.

Wicks, F. J. & Whittaker, E. J. W., 1977. Serpentine textures and serpentinization. *Canadian Mineralogist* **15,** 459–488.

Wilson, M., 1989. *Igneous Petrogenesis*. London: Unwin Hyman.

Wood, B. J., 1990. An experimental test of the spinel peridotite oxygen barometer. *Journal of Geophysical Research* **95,** 15845–15852.

Wood, B. J. & Virgo, D., 1989. Upper mantle oxidation state: ferric iron contents of lherzolite spinels by ^{57}Fe Mössbauer spectroscopy and resultant oxygen fugacities. *Geochimica et Cosmochimica Acta* **53,** 1277–1291.

Wood, S. A., 1987. Thermodynamic calculations of the volatility of the platinum group elements (PGE): the PGE content of fluids at magmatic temperatures. *Geochimica et Cosmochimica Acta* **51,** 3041–3050.

Yang, K. & Seccombe, P. K., 1993. Platinum-group minerals in the chromitites from the Great Serpentinite Belt, NSW, Australia. *Mineralogy and Petrology* **47,** 263–286.

Yu, T.-H., Lin, S.-J., Chao, P. Fang, C.-S. & Huang, C.-S., 1974. A preliminary study of some new minerals of the platinum group and another associated new one in platinum-bearing intrusions in a region in China. *Acta Geologica Sinica* **2,** 202–218 (Chinese, with English abstract).

Zhou, M.-F., Robinson, P. T. & Bai, W.-J., 1994. Formation of podiform chromitites by melt/rock interaction in the upper mantle. *Mineralium Deposita* **27,** 192–199.

Zhou, M.-F., Robinson, P. T., Malpas, J. & Li., Z., 1996. Podiform chromitites in the Luobusa ophiolite (southern Tibet): implications for melt–rock interaction and chromite segregation in the upper mantle. *Journal of Petrology* **37,** 3–21.

Zonenshain, L., Korinevsky, V. G., Kazmin, V. G., Pecherskiy, D. M., Khain, V. V. & Matveyenkov, V. V., 1984. Plate tectonic model of the South Urals development. *Tectonophysics* **109,** 95–135.

APPENDIX A

Table A1: Representative analyses (wt %) of silicates and oxides from chromitites and dunites in Kempirsai

Mineral:	OL	OL	OPX	CPX	CPX	AMP	AMP	AMP	AMP	AMP	AMP
Sample:	82-5/22	40L4	185-30	93-11/11	AZ1B	93-13/1	K1	93-11/1	AZ2B	93-37	93-24/1
	Incl	Incl	Incl	Incl	Incl	Matrix	Matrix	Incl	Incl	Dunite*	Incl
Locality:	MOF	MOF	MOF	MOF	MOF	MOF	MOF	MOF	MOF	MOF	BAT
SiO_2	42·05	42·49	56·76	54·22	56·53	50·90	48·82	46·62	53·84	47·52	41·23
TiO_2	0·02	0·05	0·03	0·03	0·03	0·27	0·38	0·44	0·32	0·22	1·36
Al_2O_3	0·00	0·00	0·16	0·62	0·50	6·40	8·96	9·45	3·72	6·64	14·43
Cr_2O_3	0·86	0·80	1·32	1·03	1·11	2·09	2·20	2·87	2·66	2·55	2·55
FeO_{tot}	3·63	2·34	1·80	1·03	0·78	1·39	2·01	1·31	1·02	1·86	2·15
MnO	0·09	0·02	0·00	0·11	0·10	0·08	0·06	0·03	0·02	0·00	0·04
MgO	53·61	53·53	39·45	18·51	18·77	22·06	21·06	21·05	23·00	22·08	23·21
NiO	0·62	1·08	0·21	n.a.	0·12	0·34	0·07	n.a.	0·21	0·21	0·24
CaO	0·01	0·00	0·20	24·11	24·46	11·78	12·67	12·54	12·13	12·56	9·88
Na_2O	0·00	0·00	0·00	0·24	0·08	1·75	2·07	3·27	1·17	2·61	3·14
K_2O	0·00	0·00	0·00	0·02	0·03	0·18	0·21	0·12	0·21	0·16	0·10
Cl	n.a.	n.a.	n.a.	n.a.	n.a.	0·00	0·00	n.a.	n.a.	0·00	0·00
Total	100·89	100·31	99·97	99·92	102·51	97·24	98·51	97·70	97·94	96·41	98·33
mg–number	96·3	97·6	97·5	97·0	97·7	96·6	94·9	96·7	97·6	95·5	95·0

Table A1: continued

Mineral:	GA	HYGA	HYGA	HYGA	CHL	CHL	CHL	SE	SE	ILM	Ca–Ti ox
Sample:	93-11	93-16	93-23	93-23	93-11	93-13	93-24	93-11	93-11	93-24	93-24
	Incl	Vein	Incl	Incl	Incl	Matrix	Incl	Incl	Matrix	Incl	Incl
Locality:	MOF	MOF	BAT	BAT	MOF	MOF	BAT	MOF	MOF	BAT	BAT
SiO_2	33·02	33·67	33·22	31·95	32·04	31·35	36·58	34·72	0·07	0·64	
TiO_2	0·90	5·88	4·24	4·82	0·02	0·08	0·03	0·16	0·01	52·91	75·11
Al_2O_3	2·76	0·23	15·02	11·09	12·68	14·70	13·09	4·51	0·03	0·03	0·62
Cr_2O_3	21·12	22·30	4·66	9·81	6·19	4·07	3·40	3·07	0·09	0·80	2·62
FeO_{tot}	4·91	0·67	1·44	1·66	1·40	0·49	3·29	2·23	1·86	31·67	1·26
MnO	0·12	0·07	0·00	0·22	0·00	0·06	0·09	0·06	0·00	14·93	0·97
MgO	0·25	0·95	0·45	0·46	33·68	34·29	34·85	38·33	38·31	0·16	1·02
NiO	n.a.	0·00	0·00	0·00	n.a.	0·78	0·06	n.a.	0·52	0·00	0·02
CaO	33·63	33·98	37·84	36·49	0·12	0·04	0·03	0·04	0·05	0·13	14·65
Na_2O	0·00	0·00	0·00	0·00	0·00	0·00	0·00	0·00	0·00	0·00	0·00
K_2O	0·00	0·00	0·00	0·00	0·00	0·00	0·00	0·00	0·00	0·00	0·05
Cl	n.a.	n.a.	n.a.	n.a.	n.a.	0·00	0·00	0·00	0·10	0·00	0·00
Total	100·31	97·10	98·58†	98·53‡	86·04	86·55	86·13	84·98	75·69	100·86	96·96
mg-number	8·3	71·6	46·8	33·1	97·7	99·2	94·9	96·8	97·3		59·2

†Includes 0·29% V_2O_3 and 0·97% excess oxygen (EDS).
‡Includes 0·16% V_2O_3 and 0·60% excess oxygen (EDS).
n.a., not analysed; OL, olivine; OPX, orthopyroxene; CPX, clinopyroxene; AMP, amphibole; GA, garnet; HYGA, hydrogarnet; CHL, chlorite; SE, serpentine; ILM, ilmenite; Ca–Ti ox, Ca–Ti oxide; Incl, inclusion in chromite; MOF, Main Ore Field; BAT, Batamshinsk-type chromitite at Stepninsk; *mg*-number, 100 Mg/(Mg + Fe_{tot}).

APPENDIX B

Table A2: Representative analyses (wt %) of platinum-group and base-metal-bearing minerals from chromitites in the Main Ore Field, Kempirsai

Mineral:	Alloy	Alloy	Alloy	Alloy	Erlichm.	Laurite	Erlichm.	$(Ir,Rh)S_2$	Cu–Ir–S	BM–Ir–S	Ni–Ir–S
Sample:	AZ3-3A	DP1/1	Conc	Conc	93-41	40Let3	MP-10	MP-3-1	55-2	DP5-8c	88-3
S	0·18	0·08	0·90	2·10	28·10	36·94	27·40	26·70	23·12	22·91	24·40
As	0·00	0·20	0·00	0·00	0·00	0·00	1·10	0·00	0·00	1·48	0·00
Fe	1·89	0·53	4·60	4·30	0·44	0·49	0·90	0·60	0·70	3·95	2·60
Ni	0·12	0·00	0·40	24·60	0·07	0·25	0·80	0·70	2·20	3·41	18·70
Cu	0·00	0·00	28·60	0·90	0·14	0·00	0·10	0·60	13·60	4·98	7·90
Co	0·00	n.a.	0·00	0·00	n.a.	0·01	n.a.	n.a.	n.a.	4·56	n.a.
Os	39·02	52·24	43·50	0·30	36·55	7·98	35·40	0·00	0·00	0·23	0·00
Ir	51·69	41·63	7·60	64·60	9·78	5·52	19·40	62·60	54·90	50·98	44·70
Ru	0·57	2·10	15·90	2·00	19·11	44·01	12·80	0·10	0·60	0·00	0·00
Rh	0·00	0·33	0·20	0·10	3·15	2·51	0·90	8·40	4·60	0·41	1·30
Total	100·60	98·73	101·70	98·90	97·60	97·70	98·80	99·70	99·72	92·91	99·60

Table A2: continued

Mineral:	Ni–Ir–S	Irarsite	Ruarsite	Ruarsite	Omeiite	Os–Ir–As	Ni–Ir–As	Mauch.	Orcélite	Millerite	Hz
Sample:	AX 2-1	Conc	93-11/5	Conc	Conc	Conc	Conc	DP 1/6	93-41	DP 5/7	180-40
S	23·30	11·60	12·10	12·30	0·20	0·00	0·00	0·62	0·08	32·61	26·18
As	0·00	24·40	31·99	29·60	45·70	14·30	24·30	47·77	36·80	0·00	0·00
Fe	2·00	0·00	0·22	0·00	0·00	0·50	1·90	0·01	0·51	3·02	0·68
Ni	14·60	0·30	0·34	1·70	0·10	0·30	46·30	51·04	64·84	61·36	72·06
Cu	5·50	0·70	0·00	0·20	0·10	0·50	0·40	0·06	0·00	0·00	0·00
Os	16·60	1·60	19·76	21·20	41·10	31·50	0·40	0·06	0·00	0·12	0·00
Ir	33·50	57·80	2·06	15·50	3·40	51·10	24·60	0·19	0·00	0·01	0·19
Ru	1·80	1·50	29·07	18·40	7·60	0·30	0·30	0·03	0·03	0·00	0·00
Rh	1·40	0·40	4·81	0·20	0·10	0·10	0·10	0·03	0·03	0·14	0·00
Pd	n.a.	0·10	n.a.	0·00	0·00	0·50	0·00	n.a.	n.a.	n.a.	n.a.
Pt	n.a.	0·60	n.a.	0·80	0·00	0·00	0·00	n.a.	n.a.	n.a.	n.a.
Total	98·70	99·00	102·24	99·90	98·30	99·10	98·30	99·81	102·29	97·26	99·19

n.a., not analysed; Hz, heazlewoodite; Conc, from mineral concentrate CuKα corrected for IrLλ interference; AsLα corrected for RuLα interference; RhLα corrected for RuLβ interference.